Report of the Task Group 186 on model-based dose calculation methods in brachytherapy beyond the TG-43 formalism: Current status and recommendations for clinical implementation

Luc Beaulieu[a)]
Département de Radio-Oncologie et Centre de Recherche en Cancérologie de l'Université Laval, Centre hospitalier universitaire de Québec, Québec, Québec G1R 2J6, Canada and Département de Physique, de Génie Physique et d'Optique, Université Laval, Québec, Québec G1R 2J6, Canada

Åsa Carlsson Tedgren
Department of Medical and Health Sciences (IMH), Radiation Physics, Faculty of Health Sciences, Linköping University, SE-581 85 Linköping, Sweden and Swedish Radiation Safety Authority, SE-171 16 Stockholm, Sweden

Jean-François Carrier
Département de radio-oncologie, CRCHUM, Centre hospitalier de l'Université de Montréal, Montréal, Québec H2L 4M1, Canada and Département de physique, Université de Montréal, Montréal, Québec H3C 3J7, Canada

Stephen D. Davis
Department of Medical Physics, University of Wisconsin-Madison, Madison, Wisconsin 53705 and Department of Medical Physics, McGill University Health Centre, Montréal, Québec H3G 1A4, Canada

Firas Mourtada
Radiation Oncology, Helen F. Graham Cancer Center, Christiana Care Health System, Newark, Delaware 19899

Mark J. Rivard
Department of Radiation Oncology, Tufts University School of Medicine, Boston, Massachusetts 02111

Rowan M. Thomson
Carleton Laboratory for Radiotherapy Physics, Department of Physics, Carleton University, Ottawa, Ontario K1S 5B6, Canada

Frank Verhaegen
Department of Radiation Oncology (MAASTRO), GROW, School for Oncology and Developmental Biology, Maastricht University Medical Center, Maastricht 6201 BN, the Netherlands and Department of Medical Physics, McGill University Health Centre, Montréal, Québec H3G 1A4, Canada

Todd A. Wareing
Transpire Inc., 6659 Kimball Drive, Suite D-404, Gig Harbor, Washington 98335

Jeffrey F. Williamson
Department of Radiation Oncology, Virginia Commonwealth University, Richmond, Virginia 23298

(Received 7 May 2012; revised 26 July 2012; accepted for publication 2 August 2012; published 25 September 2012)

The charge of Task Group 186 (TG-186) is to provide guidance for early adopters of model-based dose calculation algorithms (MBDCAs) for brachytherapy (BT) dose calculations to ensure practice uniformity. Contrary to external beam radiotherapy, heterogeneity correction algorithms have only recently been made available to the BT community. Yet, BT dose calculation accuracy is highly dependent on scatter conditions and photoelectric effect cross-sections relative to water. In specific situations, differences between the current water-based BT dose calculation formalism (TG-43) and MBDCAs can lead to differences in calculated doses exceeding a factor of 10. MBDCAs raise three major issues that are not addressed by current guidance documents: (1) MBDCA calculated doses are sensitive to the dose specification medium, resulting in energy-dependent differences between dose calculated to water in a homogeneous water geometry (TG-43), dose calculated to the local medium in the heterogeneous medium, and the intermediate scenario of dose calculated to a small volume of water in the heterogeneous medium. (2) MBDCA doses are sensitive to voxel-by-voxel interaction cross sections. Neither conventional single-energy CT nor ICRU/ICRP tissue composition compilations provide useful guidance for the task of assigning interaction cross sections to each voxel. (3) Since each patient-source-applicator combination is unique, having reference data for each possible combination to benchmark MBDCAs is an impractical strategy. Hence, a new commissioning process is required. TG-186 addresses in detail the above issues through the literature review

and provides explicit recommendations based on the current state of knowledge. TG-43-based dose prescription and dose calculation remain in effect, with MBDCA dose reporting performed in parallel when available. In using MBDCAs, it is recommended that the radiation transport should be performed in the heterogeneous medium and, at minimum, the dose to the local medium be reported along with the TG-43 calculated doses. Assignments of voxel-by-voxel cross sections represent a particular challenge. Electron density information is readily extracted from CT imaging, but cannot be used to distinguish between different materials having the same density. Therefore, a recommendation is made to use a number of standardized materials to maintain uniformity across institutions. Sensitivity analysis shows that this recommendation offers increased accuracy over TG-43. MBDCA commissioning will share commonalities with current TG-43-based systems, but in addition there will be algorithm-specific tasks. Two levels of commissioning are recommended: reproducing TG-43 dose parameters and testing the advanced capabilities of MBDCAs. For validation of heterogeneity and scatter conditions, MBDCAs should mimic the 3D dose distributions from reference virtual geometries. Potential changes in BT dose prescriptions and MBDCA limitations are discussed. When data required for full MBDCA implementation are insufficient, interim recommendations are made and potential areas of research are identified. Application of TG-186 guidance should retain practice uniformity in transitioning from the TG-43 to the MBDCA approach. © *2012 American Association of Physicists in Medicine*. [http://dx.doi.org/10.1118/1.4747264]

Key words: brachytherapy, treatment planning, dose calculation, radiation transport, commissioning, dose scoring, heterogeneities, material assignments

TABLE OF CONTENTS

I. INTRODUCTION

I.A. Problem description

Brachytherapy plays an important role in the curative management of cancers in a variety of disease sites,[1] most prominently, gynecological malignancies, breast cancer, and prostate cancer. Commonly used radionuclides include ^{137}Cs for low dose-rate (LDR) intracavitary brachytherapy; ^{192}Ir in the form of wires or seeds in ribbons for temporary LDR interstitial implants, and ^{192}Ir for high dose-rate (HDR) brachytherapy. Starting in the late 1960s with ^{125}I seeds,[2] and continuing with ^{103}Pd, and more recently ^{131}Cs, new low-energy (LE) radionuclides were introduced into clinical practice, revolutionizing the practice of permanent implantation. In conjunction with transrectal ultrasound (US) image guidance, LE permanent seed implantation is now one of the leading therapeutic approaches for the treatment of early stage prostate carcinoma. These radionuclides have practical advantages such as reduced shielding requirements and short half-lives, making them easier to manipulate and dispose of. In addition, a new type of LE brachytherapy source has been developed: the electronic brachytherapy source (EBS), essentially a miniaturized 50 kVp x-ray tube.

The 1995 AAPM Task Group No. 43 (TG-43) report,[3] and its more recent TG-43U1 (Ref. 4) and TG-43U1S1 (Ref. 5) updates, are currently recognized as the worldwide standard for LE photon-emitting brachytherapy dose calculation. The TG-43 approach has been widely adopted for HDR ^{192}Ir remote afterloading brachytherapy dose planning. Using a table-based approach that uses a geometric dose falloff model to facilitate accurate linear interpolation on a coarse grid, the TG-43 dose calculation formalism describes dose deposition around a single source centrally positioned in a spherical water phantom.[4] The current approach for estimating doses in brachytherapy treatment planning is to superpose precalculated dose distributions for single sources in water according to the pattern of the source placement and the source dwell-time. The single-source data are derived from one-time source-model specific Monte Carlo (MC) simulations or thermoluminescent dosimetry (TLD) measurements according to specifications outlined in the AAPM TG-43U1 report, and are strictly valid only for a homogeneous water phantom of the size and shape used for data derivation. This method is fast and practical in the clinic. However, the influence of tissue and applicator heterogeneities, interseed attenuation, and finite patient dimensions are all ignored. An exception is the occasional use of one-dimensional (1D) "effective path length" algorithms[6] applied to the total dose to account for applicators incorporating high atomic number (Z) shielding materials.[7,8] These algorithms are appropriate for the primary dose (i.e., dose contributed by direct, nonscattered photons), but fail to describe the scatter-dose component dependence on the full three-dimensional (3D) geometry. 3D scatter-integration, superposition/convolution, or transport-equation solution methods are required for acceptable accuracy.[9–11] In a 2009 *Medical Physics* Vision 20/20 article, Rivard *et al.* performed a review of the literature and concluded that accepted clinical dose parameters can be over- or under-estimated by at least 5% (and by as much as factor-of-10) in numerous situations.[12] Based on the energy range, they compiled a table (Table I of that paper) describing categories of clinical applications for which the current dose calculation standard would lead to significant deviations. These effects are reviewed in more detail in Sec. I.C of the present report.

In contrast, model-based dose-calculation algorithms (MBDCAs) offer the possibility of departing from water-only geometries by modeling radiation transport in nonwater media (tissues, applicators, air-tissue interfaces), resulting in a much more physically accurate reconstruction of the dose distribution actually delivered to the patient.

I.B. Report overview and rationale

Clinical application of material heterogeneity corrections in external beam radiation therapy (EBRT) is now the standard of practice for many modalities, e.g., IMRT and hypofractionated early stage lung cancer.[13] This transition has been made possible by the emergence of MBDCAs (Ref. 14) such as collapsed-cone (CC) convolution,[15] superposition-convolution,[16] MC methods,[17] and more recently grid-based Boltzmann solver (GBBS),[18,19] all of which can now be found in commercial planning software packages, as well as new treatment techniques and dose-time-fractionation schedules which require a more realistic appraisal of delivered absorbed dose. In contrast, relatively little use of heterogeneity corrections has been made in brachytherapy.

From a fundamental physics perspective, the photon interaction processes, which are dominated by Compton scattering in EBRT, are more forgiving in EBRT than for brachytherapy where the photoelectric effect dominates energy deposition for LE brachytherapy sources, and to a lesser degree for high-energy (HE) sources. Thus, the all-water approximation for dose calculations is much poorer at low ($E < 50$ keV) and intermediate (50 keV $< E < 200$ keV) energies than at high

energies (E > 200 keV). Even for intermediate- and HE photons, the scatter-to-primary ratio is at its maximum in materials of low Z and therefore appropriate 3D modeling of the scatter component is important. The cases of superficial implants and shielded vaginal applicators are good examples. Tissue composition heterogeneities could become critical for electronic HDR sources where mean photon energies are generally about 30 keV and the dosimetric points of interest or organs at risks (OAR) can be located many centimeters from the source.

In this context, the clinical introduction of advanced dosimetry algorithms beyond the current AAPM TG-43 formalism for sealed source brachytherapy dose calculations is highly desirable. While all of the issues mentioned previously can be tackled by MBDCAs, this adds a new layer of complexity to current treatment planning systems (TPS). In order to account for all sources of scatter and heterogeneities, accurate geometrical descriptions of the patient and implanted applicators, including assignment of cross sections to all media, must be provided on a voxel-by-voxel or component-by-component basis. In other words, the location and material composition of each unique geometric element considered in the dose calculation must be known. In current practice, CT images are used simply to perform anatomy delineation. For MBDCAs, the CT images will become a source of dose-calculation algorithm input data that are critical for dosimetric accuracy. Furthermore, this same information must be available for applicators, shields, and sources if intersource attenuation needs to be considered. The output of a MBDCA is highly dependent on how imaging and applicator structure information is obtained and used by the algorithm. Thus, whereas the TG-43 dosimetry formalism, despite its inherent limitations, provides the community with an intrinsic consistency in dose calculation, MBDCAs for all their advantages can lead to large center-to-center dose-calculation variations if specific guidance is not provided.

This report addresses three major issues associated with the advent of MBDCAs, namely,

(1) Choice of dose specification medium (Sec. III), because there are energy-dependent differences even when nonwater materials are included in the radiation-transport model depending on whether dose is specified to a water reference medium or the local tissue medium.
(2) Voxel-by-voxel cross-section assignment, as neither conventional single-energy CT nor ICRU/ICRP tissue composition recipes are *de facto* accurate guides for the task (Sec. IV).
(3) Commissioning procedures for MBDCAs (Sec. V).

Each section presents its own literature review, recommendations, and related topics for future research. The report is concluded (Sec. VI) by discussing changes in dose prescription that may result from transitioning from TG-43 dose computations to more realistic MBDCA dose estimates, and the uncertainties and limitations associated with MBDCAs.

These recommendations have been reviewed by members of the AAPM Brachytherapy Subcommittee, AAPM Therapy Physics Committee, the GEC-ESTRO Brachytherapy Physics Quality Subcommittee (BRAPHYQS), ESTRO-EIR, the American Brachytherapy Society (ABS) physics committee, and the Australasian Brachytherapy Group (ABG). This report has been approved and is endorsed by the AAPM, ESTRO, ABS, and ABG. While certain commercial products are identified in this report, such identification implies neither recommendation nor endorsement by the AAPM, ESTRO, ABS, or ABG. Nor does it imply that the product is necessarily the best available for these purposes. This report is intended for the experienced brachytherapy physicist and physician considering early adoption of MBDCAs.

I.C. Review of tissue and applicator material heterogeneity effects

A short review of early literature on the impact of dosimetry from taking heterogeneity effects into account is provided below. For a more in-depth review, the reader is referred to Rivard *et al.*[12] Options for dose scoring/reporting and notation are summarized in Table I. Dosimetric errors incurred with the TG-43 approach and the magnitudes of differences between the various doses listed in Table I depend on photon energy. For LE sources, the photoelectric process is dominant; differences in mass-energy absorption coefficients between various tissues and water (see Fig. 1)[20] can result in significant dose differences depending on the medium chosen for radiation transport and energy deposition.

Note that the studies reviewed in Sec. I.C.1 compare dose calculations in homogeneous water $D_{w,w}$ with results of MC simulations reporting dose to the local transport medium, $D_{m,m}$ (cf. Table I). More recent studies investigating the effect of using other media for dose reporting are reviewed in Sec. III.

I.C.1. Low energy regime, seeds, and miniature x-ray sources

Taylor demonstrated differences of up to 25% between $D_{m,m}$ and $D_{w,w}$ for breast tissue for the Xoft electronic miniature x-ray source with the dose ratio changing by nearly 25% over 5 cm.[21] For prostate tissue, $D_{m,m}$ and $D_{w,w}$ differ by 10% for ^{125}I and ^{103}Pd sources, with gradients of up to 20% over 5 cm in $D_{m,m}/D_{w,w}$.[21] Thomson *et al.* explored differences in $D_{m,m}$ and $D_{w,w}$ for a few different eye tissues for ^{125}I or ^{103}Pd seeds in the standardized eye plaques of the Collaborative Ocular Melanoma Study (COMS) and found that $D_{m,m}$ differed by up to 9% from $D_{w,w}$.[22] Chibani and Williamson evaluated the impact of tissue composition on dose distributions and dose-volume histograms (DVHs) in the prostate for ^{125}I and ^{103}Pd idealized implants.[23] For a ^{103}Pd-based preimplant plan, the dose $D_{m,m}$ delivered to 100% of the prostate volume, D_{100}, was 6% lower for a prostate modeled as soft tissue than for the same prostate modeled as pure water (i.e., as $D_{w,w}$). Carrier *et al.* evaluated the impact of prostate treatment plans with ^{125}I permanent seed implants using MC methods,[24] comparing dose distributions for a TG-43 calculation, full MC with water prostate, and full MC with realistic prostate

TABLE I. Summary of dose reporting possibilities. The notation for absorbed dose estimation at location **r** is $D_{x,\,y\,-\,Z}(\mathbf{r})$, where x denotes the choice of dose-specification medium (either water or local medium at **r**); y denotes the choice of voxel composition assignments used to perform the radiation transport calculations (either homogeneous water; all biological tissue approximated by water except for applicators and air-tissue interfaces; applicators and air-tissue interfaces with actual tissue compositions and densities); and Z denotes the choice of algorithm (either MBDCA or TG43).

	Notation	Method for dose calculation	Comment
1	$D_{\text{w,w-TG43}}$	Superposition of single-source absorbed dose-to-water distributions derived from a transport geometry consisting of a 30 cm liquid water sphere (<50 keV sources) or unbounded water medium (≥50 keV sources)	Clinical experience is with this quantity. However, intersource attenuation, applicator attenuation, tissue heterogeneities, and skin contours are all ignored.
2	$D_{\text{w,w/appl/air-MBDC}}$	MBDCA absorbed dose-to-water estimation assuming a transport geometry that realistically represents the geometry, composition, and density of applicators, sources, and air-tissue interfaces but assumes that all biological tissues, including bony tissues, are approximated by unit-density liquid water. Neglects any differences due to deviations of tissue composition from water.	A major improvement over $D_{\text{w,w}}$ because applicator shielding effects, interseed attenuation, and the influence of patient skin counter are all taken into account. These are the major effects for higher energy brachytherapy, e.g., HDR ^{192}Ir, and also for low energy brachytherapy in the presence of applicators. Ignores nonwater composition of tissue, which may dominate low-energy brachytherapy applications for some sites.
3	$D_{\text{m,m-MBDC}} = D_{\text{m,m}}$	MBDCA accounting for nonwater tissue composition and density as well as patient skin contour, applicator, and shields. Reporting dose to local medium.	Requires knowledge of patient media composition (estimated CT, see Sec. IV). Natural dose specification choice for MC, CC, or GBBS MBDCAs.
4	$D_{\text{w,m-MBDC}} = D_{\text{w,m}}$	MBDC radiation transport as in 3 but dose to bulk medium is converted to dose-to-water using cavity theory (conversion method to be indicated) or dose to water is scored.	Concern relating to conversion methods may arise at energies when sensitive target dimensions are similar to or smaller than secondary electron ranges, e.g., for low energy brachytherapy sources

tissue. For clinical treatment plans, differences of 4%–5% for D_{90} (the minimum dose deposited in 90% of the prostate volume) between MC simulations in water ($D_{\text{w,w}}$) and in prostate tissue ($D_{\text{m,m}}$) were found.[24] In a later study of postimplant dosimetry for 28 patients, Carrier *et al.* compared MC simulations using patient data (with media density set according to CT attenuation data) to clinical TG-43 calculations ($D_{\text{w,w-TG43}}$).[25] For D_{90}, the mean difference between the clinical technique ($D_{\text{w,w-TG43}}$) and the MC method ($D_{\text{m,m}}$) was 7%, of which 3% was due to tissue composition and the remaining 4% to interseed attenuation. The clinical calculation technique (TG-43 formalism) overestimated doses deposited in the prostate and OAR when compared to MC. Considerations for changing brachytherapy prescriptions are discussed in Sec. VI.C.

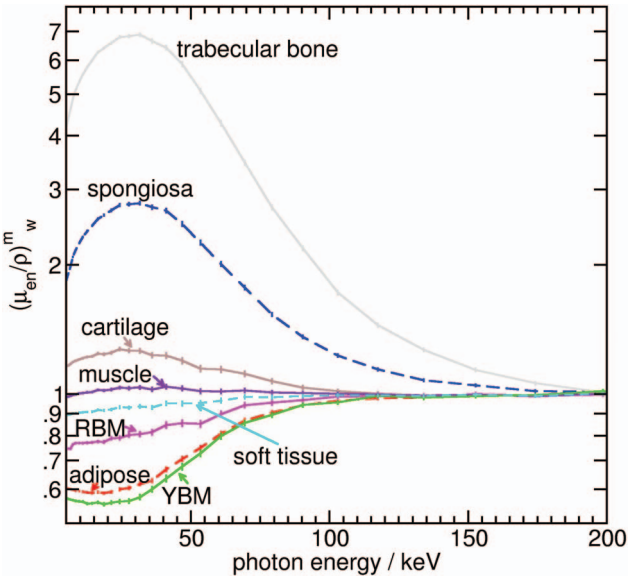

FIG. 1. Mass energy absorption coefficients for the materials indicated relative to those for water for energies from 5 to 200 keV, calculated with the EGSnrc user-code "g." Atomic compositions and densities are those from ICRU Report 44 (Ref. 20) and ICRP Report 89 (Ref. 120). The composition of the soft tissue is that for average soft tissue male (Ref. 20); the composition of the RBM (YBM) is that for "active marrow" ("inactive marrow") (Ref. 119).

Two recent studies have investigated differences between $D_{\text{m,m}}$ and TG-43 doses in the context of lung brachytherapy. Yang and Rivard investigated the effect of nonwater tissues using Monte Carlo simulations of a phantom comprised of soft tissue, lung, and cortical bone.[26] Modeling photon sources with energies between 20 keV and 400 keV, they concluded that TG-43 overestimates PTV dose and underestimates dose to bone and healthy tissue. Sutherland *et al.* performed Monte Carlo simulations with BrachyDose using patient CT data for patients treated with intraoperative ^{125}I lung brachytherapy.[27] Significant dose differences were observed between full modeling of patient tissues (calculating $D_{\text{m,m}}$) and TG-43 calculations ($D_{\text{w,w-TG43}}$); TG-43 underestimates the dose (by up to 36% of D_{90}) in larger volumes containing higher proportions of healthy lung tissue.

I.C.2. Intermediate energies: ^{169}Yb

At intermediate energies (between around 50–150 keV), effects due to varying scatter conditions are maximal for soft tissues. The differences between different media are greater

than at high energies although less than at low energies. Lymperopoulou *et al.* have shown that ^{169}Yb breast brachytherapy doses calculated with the TG-43 approach, $D_{w,w\text{-}TG43}$, can be 5% larger than MC calculated values of $D_{m,m}$ at the surface of the planning target volume (PTV), 15%–25% larger at the breast skin and 30% larger in the lung.[28] Contrast medium in a MammoSite® balloon enlarges differences with the TG-43 approach.[29]

I.C.3. Higher energies: ^{192}Ir

Anagnostopoulos *et al.*[30] reported on an esophageal ^{192}Ir brachytherapy study that showed no differences within the target region between $D_{w,w\text{-}TG43}$ and MC-calculated $D_{m,m}$, but revealed $D_{w,w\text{-}TG43}$ dose overestimations of up to 13% to the spinal cord and 15% underestimations to the sternum bone.

Lymperopoulou *et al.* showed $D_{w,w\text{-}TG43}$ calculated doses to agree with MC calculated values of $D_{m,m}$ in the PTV of an ^{192}Ir breast implant. However, doses calculated by $D_{w,w\text{-}TG43}$ were up to 5% larger than MC calculated values of $D_{m,m}$ for the skin and up to 10% larger for the lung.[28]

Poon *et al.* used the PTRAN_CT MC code to calculate $D_{w,w}$ and dose to medium $D_{m,m}$ for HDR endorectal brachytherapy with a shielded intracavitary applicator.[31,32] Two separate CT-based simulations were performed for each patient, one in which all CT voxels were assumed to consist of water and another with materials assigned according to the CT-numbers; in both cases the applicator and shielding were simulated. In soft tissues, differences between $D_{w,w}$ and $D_{m,m}$ were less than 2%. Differences between $D_{w,w}$ and $D_{m,m}$ were 18%–23% in cortical bone, 3%–3.5% in spongiosa, and 5%–7% in femoral bone.

Poon and Verhaegen found that use of $D_{w,w\text{-}TG43}$ in dose calculation for breast implants (HDR ^{192}Ir brachytherapy) overestimated the target coverage by 2% on average, and the dose to the skin by 5% relative to TG-43.[33]

I.C.4. Cone beam computed tomography

Insights into dosimetry issues for extreme tissue heterogeneities, such as bone, may be obtained from MC estimates of cone-beam computed tomography (CBCT) patient dose, since CBCT energy spectra overlap the low and intermediate brachytherapy photon-energy ranges. Ding *et al.*[34] and Ding and Coffey[35] observed that dose to bone was two to four times greater than dose to soft tissue for a Varian OBI CBCT system (40 kVp–125 kVp with mean energy of about 60 keV); these differences are expected based on the large differences in mass-energy absorption coefficients (Fig. 1). Walters *et al.*[36] reported that the elevated bone dose results in an elevated dose to bone surface cells (osteogenic cells on the endosteal surfaces), identified by the ICRP as OAR within the skeleton, due to LE electrons liberated in photoelectric events in the trabecular bone. These results indicate that skeletal doses are highly sensitive to the geometry and composition of soft-tissue cavities and bone-mineral matrix assumed, indicating that biologically relevant and accurate skeletal dosimetry is complex and may require special considerations.

II. REVIEW OF MODEL-BASED BRACHYTHERAPY DOSE-CALCULATION ALGORITHMS

This section briefly reviews model-based calculation algorithms for brachytherapy dose calculations taking into account heterogeneous geometries. While first-principles approaches (Sec. II.B) are the most accurate, the semiempirical methods reviewed in Sec. II.A address to varying degrees the clinical need for improved accuracy with high computational efficiency compared to the TG-43 method, e.g., in optimizing source placement and dwell times. A more detailed overview of calculation algorithms can be found in a 2009 *Medical Physics* Vision 20/20 paper by Rivard *et al.*[12] and in two book chapters from the 2005 AAPM/ABS Brachytherapy Summer School Proceedings.[37,38]

Collision kerma from primary photons (interacting for the first time outside the source) can be calculated using 1D ray-tracing and accurately approximates primary-photon absorbed dose under charged-particle equilibrium (CPE). CPE is valid for treatment planning of brachytherapy except very close to sources[39,40] or to metal-tissue interfaces[41,42] and hence the primary dose around brachytherapy sources can be derived with full accuracy using 1D methods. The scatter dose (dose contributed by photons interacting for a second time or more), depends, however, on the full 3D geometry and requires use of 3D scatter integration methods to be accurately estimated.

II.A. Semiempirical approaches

Methods that apply 1D ray-tracing with scaling for correcting total doses due to the presence of high-Z shields around ^{137}Cs were developed early and are also used for ^{192}Ir.[8,43] Several methods of varying complexity (none, however, being fully 3D) that separate the primary and scatter dose components have been developed using 1D ray-tracing for the primary dose calculation and estimating the scatter dose component.[11,43–50] Another approach, tested for ^{192}Ir sources,[32,51] is based on MC precalculated applicator-specific dose in water distributions aiming at accounting for high-Z shields but considering the patient to be water equivalent. An additional approach uses a TG-43 hybrid technique where MC calculations for rigid brachytherapy geometries are performed for input to conventional brachytherapy planning systems.[52–56] This technique has been performed for HDR ^{192}Ir gynecological implants, skin applicators, deep-seated breast lumpectomy cavities, and for LDR eye plaque brachytherapy planning.

These semiempirical approaches allow brachytherapy treatment plans to be generated in the same timescales observed for conventional TG-43-based plans yet with markedly increased accuracy to represent the physical implant. Dose may be determined *in* any medium *to* any medium due to the precalculated MC dose kernels.

II.B. Model-based algorithms

Model-based approaches either explicitly simulate the transport of radiation in the actual media or employ multiple-dimensional scatter integration techniques to account for the dependence of scatter dose on the 3D geometry. The three methods of current interest to brachytherapy treatment planning are CC superposition/convolution, GBBS, and MC simulations.

II.B.1. Collapsed-cone superposition/convolution method

CC is a kernel superposition method designed for treatment planning applications and optimized for calculation efficiency through angular discretization ("collapsed cones") of the kernels along a radiation transport grid.[15] The kernels map the spatial energy deposition response of scattered photons and charged secondaries for a reference medium, commonly water. The common approach in EBRT, where CC has long been used,[14] is to use two kernels, one for the primary dose and one for the scatter dose, both operating on the energy released by primary photons. In brachytherapy, the approach is to calculate the primary dose through a direct raytrace of the primary photons using the kerma approximation, and use a scatter order driven process to calculate dose from first scatter and multiple scatter separately with different kernels,[9,57–59] using the raytrace results for the primary dose as a source term for scattering. Raytracing operations are used to scale both the primary dose and all kernels for heterogeneities based on the density scaling theorem of O'Connor[60] and methods going beyond density scaling have been developed to scale kernels for heterogeneities of high atomic numbers.[58] For the primary and first scatter doses, this does not impose any approximations other than discretization effects, but is more approximate for the multiple scattering dose. The source characterization data needed for the raytracing of the primary dose can effectively be derived from precalculated primary dose distributions in water, which have motivated the suggestion of a primary and scatter separation (PSS) formalism[61] for source characterization that also provides backwards compatibility with the TG-43 tabulations. The BT collapsed cone algorithm is currently being integrated to the Oncentra Brachy TPS from Elekta (Veenendaal, The Netherlands).[62]

II.B.2. Deterministic solutions to the linear Boltzmann transport equation

Deterministic methods for solving the linear Boltzmann transport equation (LBTE) in integral or differential form yield approximate solutions that converge to the true continuous LBTE solution in the limit of very fine phase-space mesh spacing. There are several common approaches used,[63] including method-of-characteristics, spherical harmonics, and discrete ordinates.

Deterministic approaches solve the LBTE by systematically discretizing spatial (via finite difference or element meshes), angular (via discrete ordinates, spherical harmonics, etc.), and energy variables (via multigroup approximation), which results in a linear system of equations, which are iteratively solved. Because these methods are all based on phase-space discretization, TG-186 categorizes them as grid-based Boltzmann equation solvers (GBBS). Zhou and Inanc developed a GBBS, which they applied to LE brachytherapy,[64] based on direct evaluation of the integral LBTE, expanded in orders of scattering. Daskalov *et al.* applied a 2D discrete-ordinates GBBS (from DANTSYS) (Ref. 65) for the dosimetric modeling of ^{125}I and ^{192}Ir brachytherapy sources.[66,67] Further studies have been performed using the 3D Attila® radiation transport software (Transpire Inc, Gig Harbor, WA), for which a third-order linear discontinuous finite-element method (DFEM) is used for spatial discretization. Like DANTSYS, Attila® discretizes angular and energy phase-space variables via the discrete-ordinates and multigroup approximations, respectively. Mourtada *et al.* reported on Attila® dose distributions around a ^{137}Cs shielded colpostat and compared the results to MC simulations in liquid water.[68] Further optimizations and refinements were performed by Gifford *et al.*[18,69] who compared Attila® and MCNPX 3D dose distributions for ^{192}Ir and ^{137}Cs sources. More recently, Transpire Inc has created an optimized radiation-therapy specific version of the Attila® GBBS called Acuros® first for HDR brachytherapy[70–72] and later for EBRT.[19,73–75] Acuros® was introduced commercially by Varian Medical Systems (Palo Alto, CA).

II.B.3. Monte Carlo simulations

The MC simulation solves the linear LBTE by random sampling and is the current state of the art in computational dosimetry. The first MC code with an advanced geometry package specific to brachytherapy sources having several nonanalog estimators (to increase computational speed) was PTRAN.[76] PTRAN can calculate the primary dose analytically and perform MC simulations for the scatter dose part.[2,77] For treatment planning applications increasing computational efficiency through correlated sampling has been investigated.[78,79] Chibani and Williamson have presented a fast MC code intended as a dose calculation engine for LE brachytherapy seeds.[80] BrachyDose is an extension to EGSnrc allowing for use of a track-length estimator and modeling of clinical sources.[81,82] GEANT4 has also been used for postimplant treatment planning.[25] Most brachytherapy treatment planning applications are based on the assumption of CPE and implement the equivalence of absorbed dose and collisional kerma using track-length estimators, and may employ phase-space files to characterize sources before "run-time." Further references to such applications are given in Sec. III. The readers are referred to Sec VI.A for a discussion of the differences between MC and GBBS.

III. DOSE SPECIFICATION MEDIUM SELECTION

MC simulations and other MBDCA methods offer the possibility of realistic modeling of the absorbed dose distribution in patient treatment geometries, including the impact of

applicator materials, skin surface contour, and deviation of tissue composition and density from those of liquid water. As in megavoltage EBRT,[83,84] modeling radiation transport in nonwater media confronts the medical physicist with another decision: the selection of dose specification medium. Absorbed dose can be reported either to the local tissue composing each voxel, $D_{m,m}$, or to a fixed reference medium (usually but not necessarily water), $D_{w,m}$, regardless of the composition of the underlying voxels. As summarized in Table I, choices for absorbed dose estimation at location $\mathbf{r}$ may be represented by $D_{x,y\text{-}Z}(\mathbf{r})$ where: x denotes the choice of dose-specification medium (either water or local medium at $\mathbf{r}$); y denotes the choice of voxel composition assignment used to perform the radiation transport or scatter-integration calculations (cf. Table I); and Z denotes the algorithm (either MBDCA or TG-43). In the TG-43 protocol, both the transport geometry and the dose-specification medium are taken to be water:$D_{w,w\text{-}TG43}(\mathbf{r})$.

Choosing between the competing $D_{w,m}$ and $D_{m,m}$ alternatives in brachytherapy parallels the controversy this issue has engendered in megavoltage EBRT planning; arguments from the EBRT debate are briefly reviewed in the present paragraph.[83–85] For EBRT, one argument for reporting $D_{w,m}$ is maintaining consistency with earlier calculation methods that reported dose to water.[83,84] A more recent argument in support of $D_{w,m}$ reporting is that the biological targets of interest, i.e., cells or cell nuclei, consist mainly of water[85,86] and are likely to vary less between tissue types due to their functional similarity than the tissue-averaged composition. Proponents of $D_{m,m}$ for EBRT reporting argue that: $D_{m,m}$ is the quantity inherently computed with Monte Carlo simulations and some other MBDCA; that conversion from $D_{m,m}$ to $D_{w,m}$ adds unnecessary uncertainties; and that energy deposited to macroscopic regions of interest dominates complications and tumor control. The AAPM TG-105 report on MC EBRT treatment planning does not take a position in favor of reporting either $D_{m,m}$ or $D_{w,m}$;[85] however, it recommends that publications clearly state which quantity is reported and provide information to allow conversion between them. These conversions of $D_{m,m}$ to $D_{w,m}$ and vice versa employ Bragg-Gray (small cavity) theory and ratios (water to medium) of mass collision stopping powers (e.g., see review in TG-105 report[85] and recent discussion by Ma and Li[87]). With the exception of specifying clinically meaningful doses to bone,[88] the controversy regarding the medium for dose specification in EBRT is largely academic since the differences between $D_{w,m}$ and $D_{m,m}$ are limited to 2% for all soft tissues,[89–92] with similar results obtained for proton beams.[93]

Somewhat different issues need to be considered in selecting the dose-reporting medium for brachytherapy and other keV photon field applications. While secondary charged particle ranges of the order of several centimeters are common in megavoltage photon EBRT, they are much shorter in photon brachytherapy (cf. Table II). Thus, in brachytherapy, CPE is generally a valid assumption for dose calculations using common treatment planning voxel grids. Under CPE, absorbed dose equals collision kerma and can be approximated by kerma since brachytherapy energies are sufficiently low to yield negligible radiative energy losses: $D_{w,m} = K^{coll}_{w,m} \approx K_{w,m}$ and $D_{m,m} = K^{coll}_{m,m} \approx K_{m,m}$, where K^{coll} and K denote collision kerma and kerma, respectively. In EBRT, cellular and subcellular biological targets can be considered small cavities with small dimensions in relation to secondary charged-particle range; this is not generally the case in brachytherapy. In addition, LE brachytherapy dose distributions are highly sensitive to the atomic compositions of media (Fig. 1).

TABLE II. CSDA ranges of secondary electrons in unit density water [calculated with ESTAR (Ref. 94)] at selected energies relevant for brachytherapy.

Electron energy [keV]	CSDA range in water [cm]
10	2.5×10^{-4}
30	1.8×10^{-3}
90	1.2×10^{-2}
350	1.1×10^{-1}
1000	4.4×10^{-1}
3000	1.5×10^{0}

In EBRT, unrestricted mass collision stopping power ratios are often used to convert $D_{m,m}$ into $D_{w,m}$, an approach that is valid only if the water cavity is a Bragg-Gray cavity, i.e., small enough to not perturb the fluence of secondary electrons generated in the medium. Although the appropriate water volume (cavity) size remains to be determined, the Bragg-Gray assumption implies that these cavities are much smaller than the 3–5 mm-sized voxels typically used for dose calculation, e.g., cavities may represent cellular structures or micrometer-size radiosensitive targets (e.g., soft tissue structures within trabecular bone).[36,86,88] In the context of proton therapy, Paganetti discussed the conversion of dose to a patient voxel (of local medium) to dose to water for an *infinitesimal* volume of water within that voxel.[93] While $D_{w,m}$ may be computed on-the-fly for some MC dose codes, e.g., by multiplying the energy loss from each electron condensed history step by the water-to-medium ratio of restricted mass collision stopping powers, the conversion of $D_{m,m}$ into $D_{w,m}$ is typically performed as a postprocessing step which occurs after calculation of $D_{m,m}$ on a mm-sized voxel grid.[85]

The ranges of secondary electrons set in motion by photons from brachytherapy sources are generally shorter than those for EBRT and vary considerably between the different brachytherapy energy regimes (see Table II for continuous slowing down approximation (CSDA) ranges of electrons in water for electron energies between 10 keV and 3 MeV).[94] If radiation target volumes ("cavities") are considered to be macroscopic millimeter-sized voxels, then the range of secondary electrons may generally be considered short in comparison with the cavity size (for ^{192}Ir energies and below); hence large cavity theory using ratios (water to medium) of mass-energy absorption coefficients could be used for the postprocessing $D_{m,m}$ to $D_{w,m}$ conversion; direct computation of $D_{w,m}$ using the collision kerma approximation should yield identical results. While a cavity of cellular dimensions might be considered "Bragg-Gray-like" for ^{192}Ir at 380 keV or for MeV photons (EBRT), the situation is different below

50 keV: cellular dimensions are comparable to the ranges of secondary electrons (mammalian cell diameters are generally of order 10–20 μm; cell nuclei diameters range from a few micrometers to upwards of 10 μm),[95] rendering both large and small cavity theory assumptions suspect. For example, for ^{125}I sources, secondary electron ranges vary from 3 to 20 μm (Table II). Thus, depending on the size of an assumed biological target in relation to photon energy, different calculation techniques are required to compute $D_{w,m}$. In addition, for LE brachytherapy the two quantities $D_{w,m}$ and $D_{w,w\text{-}TG43}$ differ considerably regardless of the method used to compute $D_{w,m}$ (see Sec. III.A) and hence, for this energy regime, one cannot motivate reporting $D_{w,m}$ to connect with previous clinical experience. However, for HE brachytherapy sources, the situation is more similar to EBRT.

Sections III.A and III.B discuss the relationships between $D_{m,m}$ and $D_{w,m}$ in the context of cavity theory. Section III.A focuses on the large cavity regime and reviews recent publications which compare $D_{m,m}$ and $D_{w,m}$ under this assumption. This is followed in Sec. III.B with a cavity theory analysis of cellular and subcellular target dosimetry and a discussion of issues related to the choice of dosimetric medium, based on ongoing and recent research by Thomson *et al.*[96] and Enger *et al.*,[97] designed to determine which choice of macroscopic dose specification medium might better correlate with absorbed dose to biologically relevant cellular or subcellular targets. After reviewing the scientific research in Secs. III.A and III.B, Sec. III.C presents the recommendation of TG-186 on the medium for dose specification. Areas for future research appear in Sec. III.D.

III.A. Relationship between $D_{m,m}$ and $D_{w,m}$ in the large cavity regime

Recently published studies[27,98,99] comparing $D_{m,m}$ and $D_{w,m}$ either assume that $D_{w,m}$ and $D_{m,m}$ are related by the mean ratio of mass-energy absorption coefficients (water/medium), $\left(\overline{\mu_{en}/\rho}\right)^{w}_{m}$, or directly compute (under the assumption of CPE) both $D_{w,m} = K^{coll}_{w,m}$ and $D_{m,m} = K^{coll}_{m,m}$. The latter are derived by application of the mass-energy absorption coefficients for water or medium, m, to the photon energy fluence, $\Psi_m(E, \mathbf{r})$ at the point of interest, $\mathbf{r}$, found by transporting photons through the actual heterogeneous geometry

$$D_{targ}(\mathbf{r}) \approx K^{coll}_{w,m}(\mathbf{r}) = \int \Psi_m(E,\mathbf{r})\,(\mu_{en}(E,\mathbf{r})/\rho)_w\,dE = (\overline{\mu_{en}(\mathbf{r})/\rho})^{w}_{m} K^{coll}_{m,m}(\mathbf{r}) = (\overline{\mu_{en}(\mathbf{r})/\rho})^{w}_{m} D_{m,m}(\mathbf{r}), \quad (1)$$

where $D_{targ}(\mathbf{r})$ denotes the absorbed dose to the biologically relevant target at location $\mathbf{r}$. Equation (1) assumes both that this target cavity is water equivalent and that its minimum linear dimension is large in relation to the secondary electron ranges.

Large differences between $D_{m,m}$ and $D_{w,m}$ are expected for certain media at low energies based on the behavior of mass-energy absorption coefficients at low energies (Fig. 1), an expectation confirmed by recent studies.[27,98–100] Differences between $D_{m,m}$ and $D_{w,m}$ are most significant for photons below 50 keV and can be as high as 70%–80% for soft tissues, rising up as high as a factor of 7 for bone.[98–100] Landry *et al.* reported that the large cavity conversion factors for going between $D_{m,m}$ and $D_{w,m}$ (i.e., ratios of mass energy absorption coefficients) for LE brachytherapy sources (^{125}I, ^{103}Pd, ^{131}Cs, and an electronic brachytherapy source operating at 50 kV) do not vary significantly with distance from the source for distances up to 6 cm in a variety of tissues (adipose, mammary gland, prostate, muscle, skin).[98] Differences between $D_{m,m}$ and $D_{w,m}$ are within 3%–5% for soft tissues at the higher ^{192}Ir energy, rising to around 15%–25% in bone.[99]

For biological targets having dimensions on the order of 10 μm, it is only for the lowest energy sources that the large cavity theory may make biological sense.[97] For higher energy ^{192}Ir and ^{137}Cs sources, the large cavity assumption implies that targets have dimensions on the order of 1 mm and thus excludes the interpretation of the target being the cell or a part thereof.

III.B. $D_{m,m}$ and $D_{w,m}$ relationships in the small and intermediate cavity regimes

For a water-equivalent target that is much smaller than the secondary electron range, located at position $\mathbf{r}$, and surrounded by a homogeneous nonwater medium of macroscopic dimensions, the absorbed dose to the target is

$$D_{targ}(\mathbf{r}) \approx D_{w,m}(\mathbf{r}) = (\overline{\overline{S_{col}}}(\mathbf{r})/\rho)^{w}_{m} D_{m,m}(\mathbf{r}) = (\overline{\overline{S_{col}}}(\mathbf{r})/\rho)^{w}_{m} K^{coll}_{m,m}(\mathbf{r}), \quad (2)$$

where $(\overline{\overline{S_{col}}}(\mathbf{r})/\rho)^{w}_{m}$ is the average over the photon energy fluence spectrum of $\overline{S_{col}}(E,\mathbf{r})/\rho$, the mass collision stopping power averaged over the slowing-down spectrum arising from secondary electrons liberated by collisions at $\mathbf{r}$ of photons with energy E. Equation (2) was derived using the fact that $(S_{col}(E)/\rho)^{m}_{w}$ is independent of electron energy to first approximation (Fig. 2, generated using the EGSnrc user-code examin[101]). Unlike the large cavity conversion factor $(\overline{\mu_{en}(\mathbf{r})/\rho})^{w}_{m}$ [Eq. (1)], which can vary by as much as an order of magnitude from one tissue to another for LE brachytherapy (Fig. 1), the small cavity conversion factor, $(\overline{\overline{S_{col}}}(\mathbf{r})/\rho)^{w}_{m}$, deviates from unity by no more than ±5% for soft tissues over the brachytherapy energy range. Except for the very lowest energies where biological targets of the order of 2–10 μm are comparable to secondary electron ranges, Eq. (2) suggests that for kerma-based MBDCAs, $K_{m,m}$ is a more logical quantity to score than $K_{w,m}$.

A review of cellular morphology (size and composition of cellular components) reveals that nuclei and cytoplasm contain significant mass fractions of proteins, inorganic elements (ranging from sodium to calcium), and lipids (adipose cells only) and that these fractions vary widely with cell type.[96] Values of $(\overline{\mu_{en}(\mathbf{r})/\rho})^{w}_{m}$ for cytoplasm and nuclear media (for many soft tissues and tumor types) deviate from unity (up to

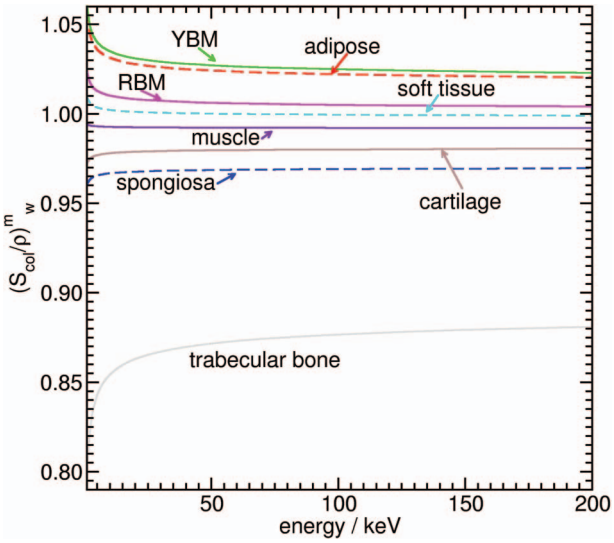

FIG. 2. Unrestricted mass collision stopping power ratios for the materials indicated relative to those for water generated using the EGSnrc user-code examin (Ref. 101). Atomic compositions and densities are the same as Fig. 1.

10%) for ^{103}Pd and ^{125}I spectra. Hence, cell targets may not generally be assumed to be water equivalent.

Enger *et al.* used Geant4.9.4 to score dose to 14 μm diameter cavities consisting of either water, cell nucleus medium, or soft tissue embedded in small phantoms composed of uniform soft tissue, to compute $D_{w,m}$, $D_{n,m}$ (where "n" represents cell nucleus medium; cells were not explicitly modeled), and $D_{m,m}$, respectively.[97] For source energies between 20 keV and 300 keV, it is reported that $D_{w,m}$ is a "good substitute" for $D_{n,m}$ for the soft tissues (breast, prostate, muscle, adipose) and the four cell nucleus compositions considered under the assumptions used in the simulations. It was concluded that there is a need for more data on tumor and healthy tissue cell compositions as doses to the cavities of nuclear media depend on their composition. Further investigations of issues related to cell dosimetry for brachytherapy likely require accurate simulation of media surrounding the nucleus as many electrons depositing dose in the nucleus are set in motion outside it. To this end, research by Thomson *et al.* involved Monte Carlo simulation of clusters of cells including cell nuclei, cytoplasm, and extracellular fluid.[96] Their results (full paper under review August 2012) suggest that doses to cell nuclei are sensitive to the presence of the different media surrounding the nucleus (e.g., cytoplasm, extracellular fluid); nuclear doses and their relation to $D_{w,m}$ and $D_{m,m}$ depend on many factors including cell and nucleus size, cellular and bulk tissue compositions, and source energy.

The complexity of the relationship between macroscopic and biological target doses is well illustrated by adipose cells. Such cells have a very large diameter, typically 100 μm, with each cell containing approximately 96% lipid, 2% intracellular water, and 2% electrolytes and protein. An idealized model of a fat cell might consist of a 33 μm thick spherical shell of lipid, enclosing a 34 μm diameter cytoplasmic cavity which in turn surrounds a 3 μm nucleus. Suppose that the relevant biological target is the nucleus. For photons with energies less than 50 keV, this is a very complex situation in which the target can approximately be modeled as a Bragg-Gray cavity, but where secondary electrons arise from photon collisions in two different compartments (lipid droplet or cytoplasm). These compartments have significant compositional differences resulting in more than a twofold reduction in the cytoplasmic $(\overline{\mu_{en}(\mathbf{r})/\rho})^{m}_{w}$ ratio in the ^{103}Pd–^{125}I energy range, with deviations exceeding 10% persisting at energies as high as 90 keV. This complex situation is reminiscent of the two-component thick-wall ion chamber problem solved by Almond and Svensson.[102] Following this approach:

$$D_{targ} = D_{nucl} \approx K^{coll}_{m,m} \times \left[\alpha \left(\frac{\overline{\mu_{en}}}{\rho} \right)^{lip}_{m} \left(\frac{\overline{S}}{\rho} \right)^{nucl}_{lip} + (1-\alpha) \left(\frac{\overline{\mu_{en}}}{\rho} \right)^{cyto}_{m} \left(\frac{\overline{S}}{\rho} \right)^{nucl}_{cyto} \right], \quad (3)$$

where D_{nucl} is the dose to the target nucleus, α is the fraction of electron fluence crossing the nucleus (=nucl) arising in the lipid shell (=lip) and (1- α) is the corresponding fraction arising from the cytoplasmic shell (=cyto). Invoking the approximations that nucl $\approx$ cyto $\approx$ wat and $m \approx$ lip, Eq. (3) becomes

$$D_{targ} = D_{nucl} \approx K^{coll}_{lip,lip} \times \left[\alpha \left(\frac{\overline{S}}{\rho} \right)^{wat}_{lip} + (1-\alpha) \left(\frac{\overline{\mu_{en}}}{\rho} \right)^{wat}_{lip} \right]. \quad (4)$$

Even in this simplistic approximation, D_{targ} is the weighted average of a correction that is as large as two with one that is approximately 0.95, with weighting factors that vary strongly with energy and cellular dimensions. An even more complex analysis would arise if one were to treat the nuclear target as an intermediate size cavity by means of Burlin cavity theory. In this scenario, only MC methods capable of transporting both photons and secondary electrons through a complete microscopic-scale geometric model could quantitatively estimate a biologically meaningful target dose. While research investigating relations between macroscopic medium dose and cellular absorbed doses and employing MC methods is ongoing,[96,97] this example clearly shows that it is premature and potentially misleading to conclude that either the small or large cavity models can be naively applied to water-equivalent targets if the goal is to maximize the correlation between the macroscopic dose descriptor and biological effectiveness.

III.C. Recommendations

The scientific literature reviewed in Secs. I.C, III.A and III.B reveals that the adoption of MBDCA for brachytherapy will generally change reported doses compared to the previous water-based dosimetry practices (e.g., following the TG-43 formalism, $D_{w,w\text{-}TG43}$), whether $D_{w,m}$ or $D_{m,m}$ is

reported. Depending on the clinical setting (source energy, treatment site, biological tissues in the region of interest), both $D_{w,m}$ and $D_{m,m}$ may deviate significantly from $D_{w,w}$ ($D_{w,w\text{-}TG43}$), as well as from each other, especially in the LE domain. Hence, it is difficult to motivate selection of dose specification medium on the basis of maximizing correlation with TG-43-era clinical dose specification. The lack of correlation of $D_{w,m}$ and $D_{m,m}$ with $D_{w,w\text{-}TG43}$ motivated the Task Group to reframe the choice of dose-specification medium from a debate over competing dose-specification conventions to a scientific question: which approach maximizes the correlation between the macroscopic dose distribution and absorbed dose to biologically relevant targets, and, ultimately, underlying biological response?

At the time of writing, it is unclear (due to the lack of published data) whether $D_{w,m}$ better tracks energy imparted to potential targets of subcellular dimensions than does $D_{m,m}$, or vice versa. Over some of the brachytherapy energy range, 3–10 μm biological targets are small cavities. Considering a simple model in which the local voxel is uniform, homogeneous (nonwater) bulk medium except for isolated biological targets of diameters much less than the secondary electron range, dose to biological targets is better tracked by $K_{m,m}^{coll}$ than $K_{w,m}^{coll}$ [Eq. (2)]. Hence, for MBDCA invoking charged particle equilibrium ($D_{m,m} \approx K_{m,m}^{coll}$), this simple model suggests that dose to biological targets is better tracked by $K_{m,m}^{coll}$ than $K_{w,m}^{coll}$. Thus, if $D_{w,m}$ is desired, it is preferable to apply postprocessing small cavity conversions rather than to erroneously invoke the large cavity approximation by directly computing $K_{w,m}^{coll}$. At the lowest brachytherapy energies where the small cavity approximation breaks down, the appropriate conversion method from $D_{m,m}$ to $D_{w,m}$ or $D_{m,m}$ to D_{targ} is unknown; nor is it known whether $K_{w,m}$ better tracks D_{targ} than $K_{m,m}$. Further, available radiobiological data suggest that water may not be the most appropriate reference medium as cellular and subcellular targets contain large and variable fractions of water, electrolytes, proteins, and lipids.

As available evidence does not directly support $D_{w,m}$, reporting $D_{m,m}$ is preferred as it is a conceptually well-defined quantity, in contrast to $D_{w,m}$, which is a theoretical construct without a physical realization in a nonwater medium. On the basis of all these considerations, it is the consensus of TG-186 to require only reporting of $D_{m,m}$ when using MBDCAs. This does not preclude individual practitioners or protocol groups from reporting $D_{w,m}$ or other quantities of interest along with $D_{m,m}$. Further, TG-186 views the required $D_{m,m}$ reporting as an interim recommendation; a definitive recommendation requires additional research, as discussed in Subsection III.D.

III.D. Areas of research

To address the underlying scientific question stated above, namely, the question of which dose specification approach maximizes the correlation between macroscopic dose and dose to biological targets, further studies on the relationship between radiobiological target doses as functions of target geometry, cellular anatomy, and tissue anatomy are needed. Through such studies, the optimal choice of dose specification medium, $D_{x,m}$, as well as a method of estimating this quantity from photon energy fluence or $D_{m,m}$ may be identified. Current efforts[36,88,96,97] use idealized cell or tissue models and coupled photon-electron MC techniques to study relations between $D_{m,m}$ and dose to biological targets. Future research should include complex multicomponent and multicellular models in which the assumptions of uniformity and target isolation (used in the discussion of Sec. III.B) break down. Investigators conducting such studies should clearly specify the conversion method used in going from $D_{m,m}$ into $D_{w,m}$. Reporting conversions from $D_{m,m}$ into $D_{w,m}$ using both stopping power ratios and mass-energy absorption coefficient ratios could be interesting since potential conversion methods probably lie somewhere between these two and likely depend on the tissue or organ in question, as well as the photon spectrum and biological endpoint. As target composition and size vary from tissue-to-tissue as well as clinical endpoint, it may be appropriate to treat dose specification as an organ- and clinical-endpoint specific $K_{m,m}$ to D_{targ} postprocessing conversion in the same spirit with which absorbed dose is converted to biologically equivalent dose (BED) using variable linear-quadratic model parameters.

Comparisons of $D_{m,m}$ and $D_{w,w\text{-}TG43}$ for different source energies and biological tissues are necessary for the recalibration of prescribed and reported doses, especially for LE sources. Investigations of doses to skeletal tissues, radiosensitive bone marrow, and to biologically important subcellular structures in adipose tissue are needed.

IV. CT IMAGING AND PATIENT MODELING

IV.A. Literature review

MBDCAs generally require assignment of interaction cross sections on a voxel-by-voxel basis to compute dose. The information is taken into account in dose calculations for HE photons by using the electron densities ρ_e (or the mass densities ρ) from CT images.[103] At high energies, Compton scatter dominates and depends mostly on ρ_e (e^-/cm^3) $= \rho N_A Z/A$. The ρ_e can be extracted by using a calibration procedure using a phantom with known composition.

In brachytherapy, the dose is administered by photons with energies <1 MeV. The lower the photon energy, the larger the differences between media in terms of mass-attenuation and mass-energy absorption coefficients due to the increasing importance of the photoelectric cross section, which is approximately proportional to the cube of Z and inversely proportional to the cube of the photon energy. Human tissues are essentially water-equivalent for dosimetric purposes for MV photon beams and HE sources such as ^{137}Cs and ^{192}Ir,[104] but not so for LE sources such as ^{103}Pd, ^{125}I, and ^{131}Cs, and EBS.[50,105–107] Hence, for accurate LE photon brachytherapy dosimetry, knowledge of tissue mass (electron) density and the atomic number distribution of the material is crucial.[108] In this report, "segmentation" is defined as the spatial delineation of different regions of a 3D image dataset and assignment of elemental compositions and mass (or

electron) densities. For brachytherapy, few studies on tissue segmentation are available in the literature because the TG-43 formalism[4] is based on a water geometry with a fixed mass density.

IV.A.1. Material characterization

Breast tissue is known to vary widely in its mix of adipose and glandular tissue. ICRU-46 (Ref. 109) lists the two tissues as mainly differing in their carbon content (glands: 33%, adipose: 60%) and oxygen content (glands: 53%, adipose: 28%). The effective atomic number, Z_{eff}, is 6.67 for average adipose tissue and 7.27 for average glandular tissue.[110] Therefore, for dosimetric purposes with LE photons adipose and glandular tissue behave very differently and it is important to be able to distinguish them. Recently, a study of several thousand women who received mammography or breast CT exams revealed a population average of about 20% for the volume breast density (VBD, defined as the fractional volume of glandular tissue), contrary to the commonly assumed 50%.[111] The study also showed that VBD ranges from 0% to 75%.

A topic that deserves special attention is calcifications in prostate and breast. Prostate calcification may be present in a significant number of patients.[39,112] Using MC simulations, a preliminary study was performed to assess the dosimetric effect of calcification in prostate.[23] The authors were unable to find a reliable reference on the composition and density of calcifications in the prostate; therefore, they used breast calcifications from ICRU Report 46 as a surrogate.[109] They reported a decrease of up to 37% in the CTV D_{90} dose metric. Another study found that the CTV D_{90} parameter was lower than estimated by up to 17 Gy (about 12% of the 144 Gy prescription dose).[25] More recent pathological measurements of calcifications in prostate have been reported.[112]

Another medium that may need to be specified accurately is the imaging contrast agent. Kassas *et al.*[113] looked at the effect of iodine-based contrast medium on dose calculations for HDR ^{192}Ir partial breast irradiation with the MammoSite® system. At 1 cm away from a 6 cm diameter balloon, they obtained a dose decrease of 5.7%. Metals and other materials used in applicators and shielding also need to be assigned correctly. This is often done by using an explicit solid model of the applicator/shielding that is added to the tissues extracted from the images. One recent example of this procedure is the MC dose calculations for a shielded colorectal cancer treatment.[31] More examples can be found in the literature.[51,114–116]

Yet another issue of potential importance is the presence of edema in the prostate and breast, and its changing influence on the dose over time.[117] Although considered to be largely water-equivalent, more studies of prostate composition and volume variation are warranted.

Recently, Landry *et al.* studied in detail the tissue composition/density sensitivity of MC dose calculations for LE brachytherapy.[118] Tissue composition reported in the literature varies depending on the reference. For example, the carbon content of breast adipose tissue, which largely determines its effective atomic number and, therefore, the fraction of photoelectric versus Compton events, has been reported to vary between 52% and 68%,[110] leading to variations in effective atomic number of 6%. Similarly, for prostate tissue the carbon content reported in the literature varies widely between 9% and 26%, leading to effective atomic number variations of only 2%.[110,119,120]

Landry *et al.* also investigated the influence of tissue composition uncertainties on dose calculations for single sources of ^{125}I, ^{103}Pd, and an EBS source.[118] Figure 3 shows the dose ratio $D_{\text{w,m}}/D_{\text{w,w-TG-43}}$, where $D_{\text{w,w-TG-43}}$ is the TG-43 water approximation and $D_{\text{w,m}}$ is the dose scored with MC techniques by transporting photons in medium, and scoring in water (i.e., $D_{\text{w,m}}$ derived under large cavity assumption). In adipose tissue, all three sources show significant dose deviations from TG-43 at the distances examined. The influence of the variation in adipose composition is also shown. In prostate, the effect is smaller but still noticeable.

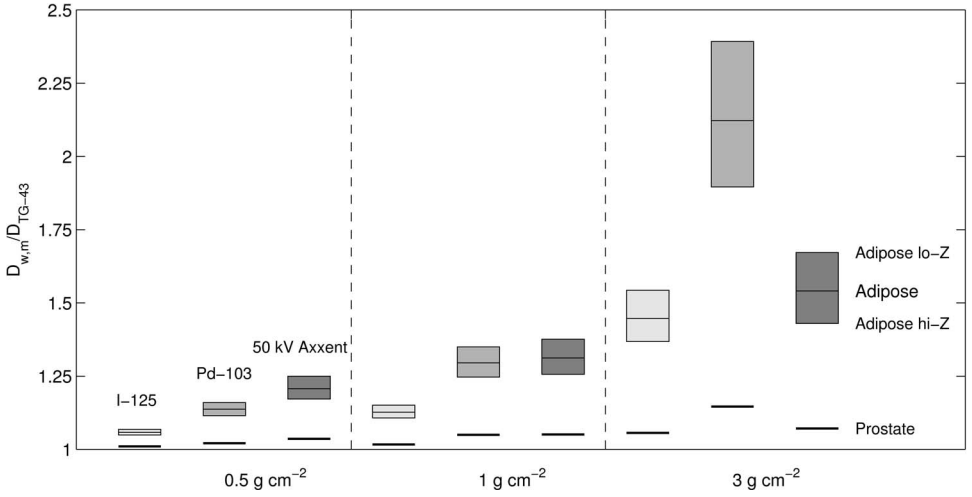

FIG. 3. $D_{\text{w,m}}/D_{\text{TG-43}}$ as a function of radiological distance for ^{125}I, ^{103}Pd, and 50 kV EBS at three different distances from a single source, using data from Landry *et al.* (Ref. 118) For adipose the vertical boxes indicate the spread in $D_{\text{w,m}}/D_{\text{TG-43}}$ with varying adipose composition.

More results are discussed in Landry *et al.*[118] For HDR ^{192}Ir brachytherapy of gynecologic cancers with standard CT/MR compatible applicators (no shielding), MDBCA has little impact (<5%) compared to TG-43 for most clinical parameters.[121,122]

IV.A.2. CT segmentation

In HE photon radiotherapy, patient heterogeneities are modeled by ρ_e derived from CT data. The accuracy of this approach depends on the reliability of the Hounsfield Units (HU), which are calibrated using tissue substitutes. The latter have to be used with care in brachytherapy as they often are designed to be tissue-equivalent only for HE photon dosimetry. In MV dose calculations, large HU errors can be tolerated before dose errors of a few percent are produced.[123,124] See also AAPM Report No. 85 by Papanikolaou *et al.*[13]

A more sophisticated tissue segmentation method has been introduced—the stoichiometric method—to take into account the atomic composition of the phantom materials used for CT calibration.[125,126] The measured HU of tissue substitutes are used to determine linear attenuation coefficients as a function of ρ_e and atomic number for the CT photon spectrum. This relationship is used to predict HU for tissues with known relative ρ_e for photon dosimetry. This method allows the patient CT data to be used directly in the treatment planning calculations without the need for segmentation and identification of specific tissue types. However, the accuracy of this method for LE photon dose calculations is unknown.

It is generally accepted that MC dose calculations are the most accurate for photon radiotherapy. The majority of MC codes require that in addition to mass or ρ_e, a medium needs to be assigned to all voxels. Media assignment errors may lead to dosimetric errors in MC and other MBDCA calculation methods, which can cause large dose errors compared to simply assigning all voxels to water with a variable density. A sensitivity study was performed for CT image use in MC dose calculations for 250 kVp–15 MV photons.[127] The authors found that inaccuracies in tissue segmentation caused dose errors of more than 40% in certain media in 250 kVp beams. These large errors occurred in $CaCl_2$ solutions, mimicking bone. Schneider *et al.*[128] showed that many different tissues have similar HU values (between −100 and +100) and hence cannot be readily resolved. They introduced a model where all skeletal tissues are composed of a mix of osseous tissue and bone marrow, and all soft tissues are a mix of fat and water. Other studies on HE photon dosimetry have been published.[129–131]

For LE photons, HU studies are rare. Watanabe derived linear attenuation coefficients from HU for LE brachytherapy MC dose calculations.[132] They introduced a model that relates HU to ρ_e and Z_{eff} accounting for both photoelectric absorption and Rayleigh scatter. Their technique led to errors of 10%–20% for the elements O, C, and Ca, and is only a moderate improvement over the older Rutherford formalism for high-Z media such as bone.[133] These authors did not investigate the ensuing effect on dose calculations.

It appears that the direct extraction of interaction coefficients for LE photons from CT images is an ill-studied subject. More accurate tissue determination may be possible with monoenergetic synchrotron x-ray CT scanners,[134,135] but this remains far from an established clinical technique. Advantages would be reduced beam-hardening artifacts and possible energy tuning to match either patient dimensions or the K-edge of a contrast medium.[134]

IV.A.3. CBCT segmentation

A similar issue is the extraction of tissue information from cone beam CT (CBCT) scanners used in the treatment room. The advantage is that information on patient geometry and composition can be obtained at treatment time, which may be different than the information at the stage of CT scanning due to various factors such as weight loss, different organ filling.[136,137] CBCT scanners have been investigated to some extent for EBRT, both for kV and MV-CBCT,[138–140] but not yet for brachytherapy. This discussion is limited to kV-CBCT as appropriate for brachytherapy. The imaging quality in a kV-CBCT scanner is inferior to a regular fan-beam CT scanner due to increased photon scatter intercepted by the larger 2D detection panel leading to reduced imaging contrast, increased cupping, and streaking artifacts.[139] Therefore, calibration of the kV-CBCT scanner in terms of HU versus ρ_e is essential for dose calculations.[138,140] On the other hand, the spatial resolution of the CBCT scanner in the axial direction is superior to a fan beam CT scanner.

A study using a kV-CBCT scanner and several calibration phantoms reported that the accuracy of EBRT dose calculations-based CBCT images of phantoms and patients was within a few percent of dose calculations based on images from a fan beam CT.[140] In contrast, more recently Hatton *et al.*,[138] also studying a kV-CBCT scanner attached to a linear accelerator, found that phantom size substantially influenced the HU. Compared to CT-based dose calculations, this led to large dose errors of up to 20% for 18 MV x-rays in bone.

In brachytherapy, the use of a CBCT scanner in the treatment room has been investigated to a limited extent, e.g., to investigate the possible use a CBCT scanner for conventional TG-43 dose to water calculations in HDR cervix treatment.[141,142] Dose to medium calculations in brachytherapy based on kV-CBCT imaging has not been attempted yet. HU calibration in kV-CBCT seems an issue that deserves more attention and CBCT images should not be used for brachytherapy dose calculations when tissue heterogeneity information needs to be taken into account.

IV.A.4. Dual energy CT and spectral CT

Nearly 40 years ago, it was proposed that dual-energy CT (DECT) may allow extraction of tissue characteristics in a more accurate way than single-energy CT.[133,143] In a similar vein, multienergy CT, or spectral CT, was recently advocated to allow more accurate tissue composition extraction.[144–146] The DECT technique is now best known for the determination of bone density.[147] It may also be used to measure arterial

calcifications,[148] or breast composition.[149] The DECT underwent steady development since its inception,[150,151] which led to research systems and clinically available products.[134,152] The DECT technique utilizes two x-ray CT images acquired using two well-separated x-ray energy spectra. This then allows obtaining an image of the mass or electron densities (i.e., morphology) and another image of the atomic numbers of the geometry (i.e., chemical composition), which greatly aids in identifying tissue types. DECT can also be used to aid extraction of photon interaction coefficients more accurately than single energy CT.[108] DECT was used to extract tissue data needed for MC treatment planning for MV and kV photon beams.[153] Spectral CT may help to extract even more tissue information than DECT.

To our knowledge, only one study attempted to use DECT for brachytherapy. The investigators proposed a method to estimate voxel-by-voxel the distribution of the photon interaction coefficients for brachytherapy energies.[108] They used two methods: a parametric fit model and a basis vector model, of which they recommended the latter. No brachytherapy dose calculations were shown in this study. Vigorous research efforts are ongoing in DECT and spectral CT.[146] It may well constitute an improvement over single-energy CT to derive tissue characteristics for brachytherapy dose calculations, but much research is needed to establish the technique for this purpose. Two recent studies showed that DECT could segment tissue phantoms more accurately than single energy CT.[154,155]

IV.A.5. CT artifacts

The CT artifacts may lead to differences between true and reconstructed photon interaction coefficients. The presence of high-Z, high-density materials in a scanned object will lead to streaking artifacts which may severely degrade image quality. Examples specifically for brachytherapy are the presence of metal applicators, vaginal packing, or radioactive seeds. Usually, those metallic objects are very close to, or even within, the target volume. Hence, without artifact correction, it is impossible to accurately assess ρ_e and the composition of some voxels. Streaks not only prevent accurate structure delineation but may also cause dose miscalculation. This is particularly true for MDBCA dose calculations in brachytherapy, which may be more sensitive to incorrect media assignment than other dose calculation algorithms.

A variety of artifact correction techniques have been developed to improve image quality. The simplest approach that can be used for minor artifacts is to correct the discrepancies in the CT images themselves.[156] More sophisticated approaches use one of three main techniques: filtered back-projection on a modified sinogram,[157–159] filtering techniques,[160] and iterative algorithms.[160–165] The modified filtered back-projection methods often involve interpolation in the sinogram domain after high-density objects have been removed. The impact on MC dose calculation accuracy was assessed for a double-hip prosthesis case.[166] For an 18 MV photon dose calculation, the dose differed significantly in the corrected and noncorrected CT geometry. This technique was also used to reduce imaging artifacts in the presence of a Fletcher-Suit applicator for HDR brachytherapy,[158,163] but these authors did not perform dose calculations. Recent studies have looked at correction methods for metallic LDR seed implants using post processing algorithms on CT slices, virtual sinogram technique, or the more efficient approach processing the raw sinogram data.[27,167–169] The presented preliminary dosimetric results indicate that artifacts can lead to large discrepancies.[27,167] It is clear that CT artifact correction should also be encouraged as a field of research to improve brachytherapy dose accuracy.

IV.A.6. Other imaging modalities

Volume delineation based on imaging modalities other than CT can be performed, especially when the lack of electron density information is not a significant problem, e.g., for a homogeneous dose calculation. Contours drawn using MRI could suffer from image distortion but can still be used successfully in brachytherapy planning [for example, prostate[170] or GYN (Ref. 171) treatments]. Image fusion with CT often offers the best results.[172] Also, US imaging has been used to outline organs in brachytherapy. In particular, transrectal US imaging is commonly used to perform LDR prostate seed implants.[173–175] This technique clearly visualizes the prostate and the urethra, but the act of imaging the organs deforms them. The consequences for dosimetry are not well understood. Three-dimensional US imaging with external US transducers offers possibilities for noninvasive image-guided brachytherapy for prostate, cervix, and breast without geometric distortion, although these techniques are currently rarely used for brachytherapy.[176,177] However, none of these techniques can presently provide information on tissue heterogeneities as would be required within the scope of the current task group report. In US techniques, contrast-enhanced imaging[178] and tissue typing[179] are active fields of research, which may also play a future role in brachytherapy.

IV.B. Recommendations

IV.B.1. Consensus material definition

The number of materials should be limited to a few. For prostate and breast, there is still disagreement on the composition to be used, so more tissue composition studies are required. The mass density derived from the CT scanner image should be used, but special measures should be taken if metal streaking and other CT artifacts are present. Table III lists the recommended tissue compositions.

IV.B.1.a. Prostate. For noncalcified prostate, the composition from Woodard and White[110] is recommended since the ICRP-1975 (Ref. 119) composition is dosimetrically equivalent to Woodard's composition. The ICRP-2003 (Ref. 120) composition refers to "average male soft tissue,"[109,118] which is similar but not the same as prostate. While individual patients may differ considerably in their prostate composition, this causes dose differences in clinical implants of only a few percent.[118]

TABLE III. Material definitions. Water is given for comparison.

Tissue	% mass				$Z > 8$	Mass density
	H	C	N	O		g cm^{-3}
Prostate (Ref. 110)	10.5	8.9	2.5	77.4	Na(0.2), P(0.1), S(0.2), K(0.2)	1.04
Mean adipose (Ref. 110)	11.4	59.8	0.7	27.8	Na(0.1), S(0.1), Cl(0.1)	0.95
Mean gland (Ref. 110)	10.6	33.2	3.0	52.7	Na(0.1), P(0.1), S(0.2), Cl(0.1)	1.02
Mean male soft tissue (Ref. 109)	10.5	25.6	2.7	60.2	Na(0.1), P(0.2), S(0.3), Cl(0.2), K(0.2)	1.03
Mean female soft tissue (Ref. 109)	10.6	31.5	2.4	54.7	Na(0.1), P(0.2), S(0.2), Cl(0.1), K(0.2)	1.02
Mean skin (Ref. 109)	10.0	20.4	4.2	64.5	Na(0.2), P(0.1), S(0.2), Cl(0.3), K(0.1)	1.09
Cortical bone (Ref. 109)	3.4	15.5	4.2	43.5	Na (0.1), Mg (0.2), P (10.3), S (0.3), Ca(22.5)	1.92
Eye lens (Ref. 109)	9.6	19.5	5.7	64.6	Na(0.1), P(0.1), S(0.3), Cl(0.1)	1.07
Lung (inflated) (Ref. 109)	10.3	10.5	3.1	74.9	Na(0.2), P(0.2), S(0.3), Cl(0.3), K(0.2)	0.26
Liver (Ref. 109)	10.2	13.9	3.0	71.6	Na(0.2), P(0.3), S(0.3), Cl(0.2), K(0.3)	1.06
Heart (Ref. 109)	10.4	13.9	2.9	71.8	Na(0.1), P(0.2), S(0.2), Cl(0.2), K(0.3)	1.05
Water	11.2			88.8		1.00

IV.B.1.b. Breast. Breast tissue is a nonuniform mixture of two distinct tissues: adipose and gland. It is clear from the literature[118] that both tissues also have their own range of compositions. If the adipose and glandular regions can be distinguished then each region can be assigned to the respective media as recommended in Table III. With current CT technology this may not always be feasible. If the adipose and glandular regions cannot be distinguished reliably, a single mean composition (for noncalcified breast) is recommended for the whole breast, corresponding to the mean gland and adipose compositions reported in the literature (Table III). From the breast CT HU, the mean overall breast density may be extracted from which the relative mass fractions of adipose and glands may be derived (see Sec IV.B.2). Using a generic breast composition is not recommended due to the large spread in breast tissue composition in the population.[180,181] If no information at all can be extracted from the CT images, then we recommend using a 20% glandular/80% adipose composition (fractions by weight) as a population average.[111]

IV.B.1.c. Calcifications. The literature is sparse on the composition of calcifications as may be present in breast and prostate. Chibani and Williamson performed MC calculations for calcified prostate.[80] They assumed that prostate calcifications are similar to breast calcifications for which they used the composition reported by the ICRU 46 report.[109] This report lists as constituents of breast calcifications hydroxyapatite, tri-calcium phosphate, and protein (e.g., their Table 2.1). From this, Chibani and Williamson listed as the elemental composition and their weight fractions H (0.3%), C (1.6%), N (0.5%), O (40.7%), P (18.7%), and Ca (38.2%) with an average density 3.06 g/cm^3.[80] If another calcification composition assignment is made, then it should be clearly reported.

IV.B.1.d. Other materials. Table III gives a few more examples of recommended tissues, listed with their mean composition; data for other media can also be found in Woodard and White[110] and also in ICRU Report 46.[109] However, we recommend that any other tissue compositions not shown in Table III be taken from the ICRU 46 report, until more detailed and accurate tissue composition data become available to the community.

IV.B.1.e. Applicators, sources, and other devices. MBDCAs require explicit specification of geometry, atomic composition, and density of all nonwater materials, including the internal structure of sources and applicators that can influence the dose distribution. In contrast, the end user of TG-43 single-source dose distributions need not directly validate the source geometry used by a MBDCA since source structure is implicitly included in the dose-rate measurements and MC calculations from which the TG-43 parameters are derived. As long as single-source MBDCA calculations are carefully validated against published TG-43 models, one can consider the MBDCA geometric assumptions indirectly but adequately validated. However, because reference-quality dose-rate distributions for each potential source-applicator combination are lacking, indirect dosimetric validation of MBDCA shielded applicator geometries is not a feasible strategy. The possibility that source and applicator geometry models in the planning system may not accurately describe the devices actually used in the clinic creates new and highly significant error pathways. This may affect treatment outcomes of many patients to the extent that completely ignoring source/applicator geometries could be less deleterious than making clinical decisions based upon inaccurate models. To guide both vendors and early adopters of MBDCAs, the Task Group makes the following recommendations:

(1) It is the responsibility of the end-user clinical physicist to confirm that MBDCA dose predictions are based upon sufficiently accurate and spatially resolved applicator and source models, including correct material assignments, to avoid clinically significant dose-delivery error prior to implementing the dose algorithm in the clinic.
(2) Patient CT grids, which typically have cubic spatial resolutions no better than 1 mm, are not adequate for accurate modeling on the spatial scale of brachytherapy sources and applicators. Dose distributions from LE sources are particularly sensitive to

simplistic geometric approximations. MBDCA vendors should use analytic modeling schemes or recursively specify meshes with 1–10 μm spatial resolution as required to accurately depict LE seed geometry. Otherwise, nuances of seed geometry will be lost and resultant dose distributions will be in error.

(3) With regards to MBDCAs, the Task Group takes the position that it is the responsibility of the manufacturers of seeds and applicators to disclose their geometry, material assignments, and manufacturing tolerances to both end users and TPS vendors (if responsible for data entry and maintenance), as this information is needed to accurately model dose around these devices. The device vendor disclosure must have sufficient detail to enable the end user to verify correct entry into the TPS. Furthermore, it is the responsibility of the TPS vendors to incorporate the device in the system or provide a simple means to the end user to do so.

(4) Prior to accepting a device vendor's disclosed source or applicator geometry for clinical application, it must be verified by an independent investigator (as defined by TG-43U1). As described by TG-43U1 appropriate verification techniques include transmission radiography and autoradiography, direct mechanical measurements, microphotography of disassembled applicator/source components, and electron microscopy of source components. MC parametric studies can be used to assess significance of geometric uncertainties.[165,182,183] If a peer-reviewed publication of the applicator or source geometry of interest is not available, the responsibility for performing the independent assessment falls to the end user.

(5) TPS vendors are nowadays increasingly providing libraries of applicators, which will ease the verification task. When such libraries are provided, it is the responsibility of the vendor to also provide visualization or reporting tools that enable the end user to verify the correctness of each included applicator and source model against independent design specifications. In addition, TPS vendors must disclose sufficient information to the user regarding the model or recursive mesh generation to allow verification of the spatial resolution requirement specified in recommendation (2).

(6) For each individual source model used clinically, during commissioning, the end user should compare MBDCA single-source dose distributions in water to directly calculated TG-43 benchmarks as described in Sec. V.B. TPS vendors should disclose the dose calculation grid sizes used and provide tools to correct for volume averaging near sources so that unambiguous comparisons between TG-43 and MBDCA dose distributions can be performed.

It is the intention of the joint AAPM/ESTRO/ABG Working Group on MBDCA to provide benchmarking data on a registry to assist with the verification process as stated in Sec. V.C.2.

IV.B.2. Material assignment method

For any application of brachytherapy dosimetry in nonwater media, tissue composition is required to compute dose. For a given organ, it is recommended that the tissue composition assignment be guided by contours approved by the radiation oncologist. In case CT images are available, for all voxels inside a given contour we recommend using the CT derived densities with a uniform tissue composition. TG-186 recommends the mean tissue compositions listed in Table III. These should be used whenever possible. In case different compositions than the recommended ones in Table III are used, calculations should also be provided with the recommended compositions to allow intercomparisons.

In any publication for which the results depend on material heterogeneities, each material composition must be specified and its origin described, e.g., citation from the literature or the authors' determination. For each material, either the mass density assumed shall be specified, or if derived from CT imaging (recommended approach), the scanner calibration method and HU-to-density and/or composition conversion technique shall be described. For the latter, the CT calibration curve depends on the CT x-ray tube kV value that is used; the appropriate calibration curve for the kV used to record the images shall be reported. However, before relying on CT-to-density conversions clinically, the confounding influence of residual streaking artifacts must be ruled out. If imaging artifacts are present, we recommend a complete override of the tissue in question with a uniform density, which may be the average of neighboring pixels. For prostate seed brachytherapy, it may be prudent to rely on the density from a preimplant CT that is free from metal artifacts.

Typical CT simulators have calibration curves for HU versus electron density relative to water, $\rho_{e,rel}$, with the latter defined as

$$\rho_{e,\,rel} = \rho N_g/(\rho N_g)_w, \tag{5}$$

where N_g stands for the electron density per unit mass (#e-/g), and the subscript w denotes water. Since N_g for bodily tissues, taken from ICRP23 (Ref. 119) and listed in Schneider *et al.*,[126] vary little over the whole range of human tissues (standard deviation 2%), the relationship between ρ and $\rho_{e,rel}$ is nearly linear. When all the tissues (excluding "inflated lung") are fit to a straight line, the following relation is obtained:

$$\rho = -0.1746 + 1.176\rho_{e,rel} \quad (R^2 = 0.99992), \tag{6}$$

which has a maximum error of less than 1% ($\rho_{e,rel}$ is dimensionless, ρ is in g cm^{-3}). For "inflated lung" usually $\rho = 0.26$ g cm^{-3} or $\rho_{e,rel} = 0.26$ is used.

A possible exception to filling structure contours with a single uniform tissue might be breast. If adipose and glandular tissues can be distinguished in the CT images, e.g., by a thresholding algorithm, or by registration with another imaging modality, the regions segmented as either adipose or gland may be assigned with their proper mean composition (Table III) and voxel mass densities.[181,184] If the adipose and glandular regions cannot be distinguished reliably, then the whole breast should be assigned to a uniform medium, which

should be a mix of adipose and gland, since it is well known that a wide, age-dependent range of mixes exists among the female population.[111] From the breast mean mass density ρ obtained from the CT scan and the known (or assumed) mean mass densities for adipose ρ_A and glandular tissue ρ_G (Table III), the fractional weight of glandular w_G and adipose tissue w_A can be estimated from

$$w_G = (1 - \rho_A/\rho)/(1 - \rho_A/\rho_G), \quad (7)$$

$$w_A = 1 - w_G. \quad (8)$$

Although a mean breast density ρ is used to determine the fractional weight composition, the CT-based voxel mass densities are recommended.

Bone, possibly comprising bone marrow, is a special case with many possible compositions. Voxel mass density should be taken from CT images. The composition of cortical bone in Table III is recommended, but it should be pointed out that bone rarely plays an import role in brachytherapy dose calculations. In case another composition is used, it should be documented and a comparison with the composition of Table III should be provided for intercomparison purposes.

In case CT images are available, for all voxels outside contours, we recommend using the CT densities with a composition of "mean soft tissue" as defined in Table III. If adequately visualized and segmented, fat-like tissues can be contoured and used in the calculation. The mean adipose tissue listed in Table III may be used; if an alternative composition is used it should be documented.

IV.B.2.a. Use of other imaging modalities. In case no CT images of the target geometry are available, the Task Group recommends:

- Using bulk tissue densities and compositions recommended previously based on contoured organs if possible.
- For LE brachytherapy, if US images are used (e.g., prostate seed implants), tissues outside the prostate contours should be set to mean soft tissues as described previously.
- For a multiple source implant, individual sources should be modeled.
- For HE sources (e.g., ^{192}Ir), MRI and US images can also be used provided that caution is exercised when extracting contours because of possible image distortions (MRI) and the nonquantitative nature of the image content. Furthermore, all tissues could be set either to the recommended bulk tissues densities and compositions from contours or alternatively to water with unit mass density. However, high-Z materials, such as applicators, should be taken into account as described in Sec. IV.B.1 and low-density media such as air must be included in the calculation to account for scatter conditions.

Finally, it is expected that TPS vendors will provide easy-to-use or automated tools to help clinical users accomplish these tasks.

IV.B.3. CT/CBCT artifact removal

For MBDCA dose calculations, it is recommended to first remove visible artifacts. In the simplest approach, a manual override of the tissue composition and density (see "Use of other imaging modalities" above) should be performed and documented. The use of advanced algorithms for artifact removal, as described in Sec. IV.A.5, is not the standard of care and should be used cautiously. For any application, the user shall clearly describe the CT artifact removal method used, if any.

IV.C. Areas of research

IV.C.1. Determination of tissue composition

The consensus list of tissue composition and density needs to be validated and refined. It needs to represent the tissues from typical cancer patients more accurately than the poorly validated recommendations from ICRU, ICRP, and other groups. Further experimental investigation into tissue compositions, including their interpatient and intraorgan variations, with an emphasis on dosimetric applications, is strongly encouraged. Research is needed to characterize prostate and breast calcifications more accurately. Tissue composition of organs in cancer patients and healthy subjects may not be the same. Ideally, the tissue composition and mass density of all voxels should be known for individual patients. With the current state-of-the-art in CT imaging, this has not yet been realized. Hence, further research into more sophisticated CT imaging methods such as dual-energy or spectral x-ray imaging and diffraction imaging is needed. Research into alternate quantitative imaging methods such as MRI and US is also needed.

IV.C.2. Segmentation methods

Research efforts are ongoing in DECT and spectral CT. Whether this constitutes an improvement over single-energy CT to derive tissue characteristics for brachytherapy dose calculations remains to be seen.[154,155] HU calibration in kV-CBCT is an issue that deserves more attention before CBCT images can be used reliably for brachytherapy dose calculations taking tissue heterogeneities into account. Tissue segmentation methods based on feature recognition and/or anatomy atlases should also be pursued in brachytherapy.

IV.C.3. CT artifact removal

It is clear that robust CT artifact correction algorithms are needed for accurate LE brachytherapy MBDCA dose calculations. Most efforts have been devoted to improving image quality and pattern recognition. Specific research efforts for improving dose calculations are needed. These methods are not yet commonly available and their potential to improve dose accuracy needs to be established.

V. MBDCA COMMISSIONING

The commissioning of a brachytherapy TPS includes tasks outlined in the AAPM TG-40, TG-56, and TG-64 reports with specifics provided on HDR ^{192}Ir systems and LDR permanent prostate brachytherapy covered in TG-59 and TG-64, respectively.[39,185–187] The majority of these recommendations address treatment-specific QA tasks, and all of these reports presume the AAPM TG-43 formalism.[3,4] As the focus of this report is advanced brachytherapy dose calculation algorithms, this section will therefore focus only on QA tasks related to MBDCAs. Commissioning brachytherapy MBDCAs will have many aspects in common with TG-43-based systems, but will require algorithm-specific tasks described below.

V.A. Literature review

The literature is growing on MBDCAs and the dosimetric effects supporting their use for certain disease sites. However, to our knowledge, there is currently little literature providing quantitative information or practical guidance on the commissioning of brachytherapy MBDCAs for clinical use.[70–72] Consequently, there is an opportunity to establish uniform commissioning procedures for various MBDCAs and across institutions.

V.B. From TG-43 to MBDCA-based commissioning

The AAPM, ESTRO, ABS, and ABG recommend minimum commissioning standards that are designed to evaluate MBDCAs under conditions similar to those encountered in clinical brachytherapy practice, based on the established TG-43 dose calculation formalism and the new MBDCA. In this section, two levels of commissioning tests that should be performed in addition to TPS QC/QA recommendations already in place based on societal guidelines are described.

All code implementations of MC, CC, or GBBS methods as MBDCA dose engines involve compromises between computational speed and sufficient dose calculation accuracy and, therefore, the resulting solutions will have a certain amount of uncertainty. These code implementations must be carefully benchmarked against MC or experimentally when uncertainties adequately permit to ensure sufficiently accurate dose prediction within the intended domain.

V.B.1. MBDCA commissioning level 1

The AAPM TG-43 dose calculation formalism is based on the assumption that photon-emitting brachytherapy sources are cylindrically symmetric, enabling single-source dose distributions to be parameterized as functions of radial distance r and polar angle θ from the source long-axis in spherical, homogenous water phantoms having outer radii R of 15 cm and 40 cm for LE and HE photon emitters, respectively. Analogous to current TPS based on the TG-43 formalism, any TPS using a MBDCA should allow direct dose or dose rate comparisons using the same dose grid size of TG-43 to facilitate direct evaluation. The clinical medical physicist should determine agreement of MBDCA TPS-derived absolute dose or dose rate in comparison with the dose or dose rate produced in the TPS using the AAPM consensus TG-43 dosimetry parameters for a given brachytherapy source model. Furthermore, hand calculations should be performed for several points-of-interest covering the range of r and θ to be used in clinical practice. As recommended in the 2004 AAPM TG-43U1 report, a 2.0% tolerance should be used for agreement with AAPM consensus TG-43 dosimetry parameters. Any deviations >2.0% should be carefully examined (see Example 1), and the clinical impact understood and documented before patient use.

A direct comparison of the MBDCA-based TPS output in a reference-sized homogenous water phantom to AAPM consensus data is helpful for physicists during transition to MBDCA-based TPS. Calculations should be conducted under reference conditions, i.e., water medium providing full scatter conditions,[99,188] at distances up to 10 cm away from the source. Comparing TG-43 dosimetry parameters is a necessary first step since these parameters describe the spatial dose distribution due to the physical source model without significant consideration of the surrounding environment. An example of this comparison is shown below.

Example 1:

Mikell and Mourtada reported on the dose distributions of a HDR ^{192}Ir source in a homogeneous water geometry calculated using BrachyVision (BV) TPS (BrachyVision v8.8, Varian Medical Systems, Palo Alto, CA) with the MBDCA-based Acuros® system.[71] The percent dose difference (%ΔD) of GBBS was determined for three cases:

(1) published TG-43 data,[189]
(2) MCNPX simulations of the model VS2000 HDR ^{192}Ir source centered in a spherical water phantom of radius $R = 15$ cm, and
(3) output from a TG-43-based TPS using vendor supplied $F(r, \theta)$ tables.

Dose differences >20% between Acuros® and TG-43-based dosimetry near the source delivery cable were observed. This was attributed to Acuros® using a 0.1 cm long delivery cable, while the TG-43-based TPS algorithm used data based on a 15 cm long cable. While these dose differences were large near the cable, the impact on clinical outcomes was negligible with dose differences of less than 3% reported.

V.B.2. MBDCA commissioning level 2

Brachytherapy treatment planning that accounts for radiation scatter conditions and the radiological influence of material heterogeneities differing from liquid water is beyond the AAPM TG-43 dosimetry formalism. However, these effects are real and potentially produce clinically relevant differences between calculated dose distributions of TG-43-based and MBDCA-based TPS. Consequently, tests of these effects on TPS results are required. Comparisons of the 3D dose distributions calculated with the clinical MBDCA-based TPS on specific virtual phantoms mimicking clinical scenarios should

be independently verified against benchmark dose distributions derived from the same phantom geometries. Based on the TPS dose output type, $D_{m,m}$ or $D_{w,m}$, the independent dose calculation should be consistent with the TPS style option. At this time, clinical physicists should be aware that such benchmark dose distributions should only be obtained via the use of a well-documented MC code. Direct comparison of the MBDCA output to a reference treatment plan having identical heterogeneous conditions is mandatory for physicists to commission MBDCA-based TPS.

For LE photon-emitting brachytherapy sources such as ^{125}I, the influence of radiation backscatter is often negligible in comparison to the impact of varying tissue composition. For HE photon-emitting brachytherapy sources, such as ^{192}Ir, radiation scatter plays a major role. While variations in soft tissue composition cause minimal changes in dose calculation, applicators having components with mass density >2 g/cm^3 are dosimetrically important. For both energy regimes, any deviations between the MBDCA-based TPS results and the reference treatment plan should be documented, and the clinical significance understood. Example 2 for LE sources, and Examples 3 and 4 for HE sources, illustrate comparisons between reference (MC-based) treatment plans and MBDCA-based TPS results.

Example 2:

Dose distributions around the 16 mm COMS eye plaque, using a fixed geometry of ^{125}I seeds, have recently been examined by two independent groups.[22,190] Both investigation teams calculated 3D $D_{m,m}$ dose distributions accounting for plaque material heterogeneities, but set the eye composition to liquid water. Dosimetric agreement on the plaque central-axis between these groups has recently been shown to be 0.991 $\pm$ 0.019 ($k = 2$).[191] The data of Melhus and Rivard were entered into the Pinnacle TPS using a MBDCA with a hybrid TG-43 MBDCA approach assuming cylindrically symmetric plaque dose distributions.[54] The TPS agreement with the reference data was 0.999 $\pm$ 0.004 ($k = 2$) for distances ranging from 0.0 to 24.3 mm from the plaque/eye interface along the plaque central-axis.

Example 3:

Zourari *et al.* tested a MBDCA-based TPS (Acuros®) to account for the altered scatter conditions generated by the proximity of a HDR ^{192}Ir brachytherapy source to the boundary of a $R = 15$ cm water phantom in comparison to MC results.[70] Dose distributions with the source shifted 5 cm and 12.5 cm from the phantom center differed by more than 20% in comparison to the TG-43 results, but showed agreement within 3% ($k = 2$) of MC results, with the largest errors along the source long-axis.

Example 4:

Petrokokkinos *et al.* reported on the dosimetric validation of Acuros® for multiple ^{192}Ir source dwell position brachytherapy applications employing a shielded applicator in homogeneous water geometries.[72] Seven VS2000 HDR ^{192}Ir source dwell positions and a partially shielded applicator (GM11004380, Varian Brachytherapy, Charlottesville, VA) were compared to corresponding MC simulation results, as well as experimental results obtained using the VIP polymer gel-MRI three-dimensional dosimetry method with a custom-made phantom. The TPS and MC dose distributions were found in agreement, mostly within 2%. However, differences between the TPS and MC results (>2%) were observed at points in the penumbra of the shields (i.e., close to the edges of the "shielded" segment of the geometries). These differences were experimentally verified and therefore attributed to the TPS. Apart from these regions, experimental and TPS dose distributions were found in agreement within 2 mm distance-to-agreement and 5% individual point dose difference criteria.

V.B.3. MBDCA commissioning workflow

New clinical tools often require new workflows for proper integration into clinical practice. Figure 4 illustrates how one might perform MBDCA validation. It should be noted for the early adopters of MBDCAs that test cases as proposed in Sec. V.B.3.a below might not be available, hence, users should perform their own verifications using independent methods (experimental or theoretical) to verify the MBDCA dose results under situations similar to the clinical situation, for example, for partial breast irradiation with MammoSite® (Hologic Inc., Bedford, MA) vs SAVI® (Cianna Medical, Aliso Viejo, CA) applicators, which is different than gynecological cases using shielded colpostats or cylinders.

V.B.3.a. Test case plans and data availability. Test case plans should be made available beyond the scientific, peer-reviewed literature via the web. This could be accomplished

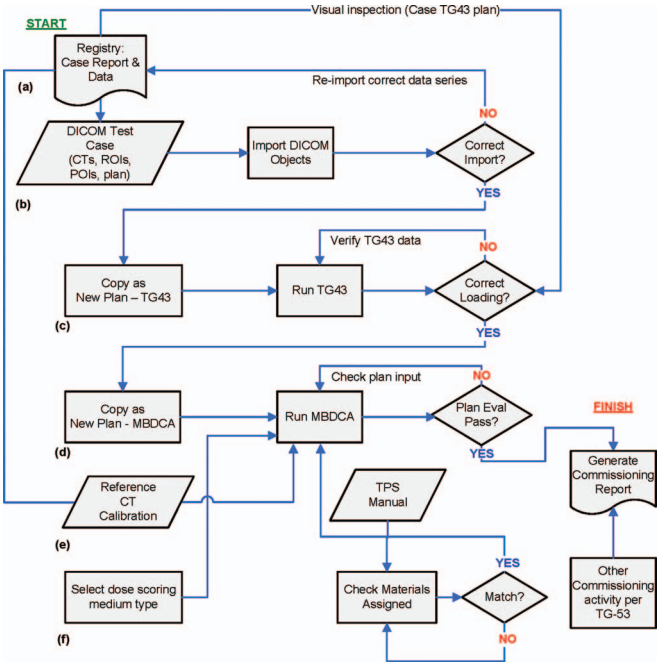

FIG. 4. MBDCA commissioning workflow for heterogeneous dose distributions calculated by a MBDCA-based TPS. Major process flow components (a)–(f) are discussed in the text.

through expansion of the joint AAPM/RPC Brachytherapy Source Registry as described by Rivard *et al.*[99] This Registry currently houses a list of sources (both LE and HDR ^{192}Ir), which meet the minimum dosimetric prerequisites and calibration frequencies recommended by the AAPM. This Registry, or some complementary international counterpart, should be expanded to include quantitative data on brachytherapy source benchmarks in easily accessible electronic format to facilitate comparisons with TPS outputs from MBDCAs beyond the current approach of pointing medical physicists to the published literature. Further, test cases should be developed with uniformity amongst vendors (when appropriate) for inclusion in their commissioning test procedures to depict dose calculations with and without MBDCAs. However, such development is beyond the scope of this Task Group and is left as an area of research (Sec. V.C).

Having an independent repository to house the reference data (such as the Registry) would help facilitate this process efficiently—especially with international accessibility. By submitting engineering drawings of the source and source-applicator combinations, manufacturers will facilitate accuracy and ease of simulations to raise the standards for brachytherapy dose calculations.

V.B.3.b. DICOM test case importing. During the MBDCA TPS commissioning process, the physicist downloads and imports DICOM files of virtual phantoms as test cases (see above) from a secure website. Such files include the geometry, precontoured DICOM-RT ROIs, points-of-interest (POIs), the RT-Plan, explicit material definitions (for cross-section assignments) and a description of the source strength, dwell positions, dwell times, and other information as found in the DICOM-RT structure.

V.B.3.c. TG-43-based dose calculation tests. Once the test case plan is imported, the first step is to copy the plan for comparison under TG-43 conditions. Reported POI results should be quantitatively compared to the plan report obtained from the Registry. This step allows for verification that all treatment plan parameters, such as source strength, loading configuration, match the test case plan prior to running the more complex MBDCA dose engine.

V.B.3.d. MBDCA-based dose calculation tests. After the initial TG-43 plan verifications, the physicist copies the test case plan and reruns the dose calculation using the MBDCA. Using the TPS plan evaluation tools, comparisons between the reference data and the institutional results are made of ROI DVHs, POI doses, etc. If the MBDCA-based TPS allows users to insert a solid brachytherapy applicator in a plan, the physicist should use the TPS measuring tools (distance and angle rulers) to compare vendor drawings to the outer and inner dimensions in the applicator library. At a minimum, the physicist should measure a few dimensions of the applicator(s) used in the clinic with mechanical calipers or radiographic imaging.[186] Given established tolerances, the physicist will release the system for general clinical use or inclusion in cooperative clinical trials.

V.B.3.e. Reference CT scanner calibration data. An important input for the MBDCA-based TPS is the reference CT scanner calibration function, especially for LE brachytherapy sources as discussed in Sec. IV. The physicist should copy this calibration curve from the Registry for TPS entry. This is not intended to replace the institution's CT calibration curve but is only for the purpose of comparing to the reference datasets. Also, the physicist should verify that the materials used in the TPS are consistent with those provided in the test case.

V.B.3.f. Select dose scoring medium type. User should specify dose scoring medium (to medium or water) following the recommendation of Sec. IV.

V.C. Areas of research

V.C.1. Workflow

The recommended commissioning workflow is general enough to be applicable to any MBDCA TPS. It contains multiple checks against the current, well-known TG-43 standard to ensure consistency of the process. However, commissioning of a MBDCA currently represents a particular challenge on multiple counts. Presently, there is only a single commercial MBDCA-based TPS available, Acuros®.

V.C.2. Test cases

It is not reasonable to validate MBDCA implementation for all possible combinations of source-applicator-geometry. Thus, exploring MBDCA limitations is an important undertaking among early adopters,[70–72] and must be expanded to various tumor sites and treatment geometries. It is expected that this exercise will be repeated for other MBDCAs as they become available. In this regard, creation of a Registry (proposed previously) should help early adopters as well as clinical medical physicists. Developers of new test cases are strongly encouraged to share their validation geometries through the Registry. To achieve this goal, TG-186 recommends creation of a Working Group with international membership. This Working Group will determine the submission modality or prerequisites, review submission prior to availability and *propose* a first set of test cases to help the community in this crucial process.

V.C.3. Gamma-index comparisons

It will be critical to refine the dose accuracy tolerance requirements for MBDCAs. The gamma-index concept (concurrently evaluating percentage agreement and distance-to-agreement) has been used for several years in EBRT dosimetry quality analysis.[192,193] Considering a gamma-index metric for brachytherapy dosimetry is an important first step. A simple ±2% tolerance level dates from 1994.[185] The 2004 AAPM TG-43U1 report further recommended a 2% tolerance for agreement of reference dosimetry parameters and overall dose calculation.[4] However, a tolerance criterion has not been specified for the distance-to-agreement between the reference dataset and that being evaluated. Further, an explicit method for performing this evaluation over the range of all clinical points of interest was not specified.

Since then, a number of investigators have applied the gamma-index concept to brachytherapy. Yang *et al.*[56] compared MC dosimetry results for HDR ^{192}Ir breast applicator to those obtained using a TG-43 hybrid MBDCA approach and found a 99.24% gamma-index pass rate with 1% and 1 mm criterion, and a 99.95% pass rate for a 2% and 2 mm criterion. Petrokokkinos *et al.*[72] examined the accuracy of the Acuros® system in comparison to MCNPX-based MC simulations for the dose distribution from a HDR ^{192}Ir source in the presence of a shielded vaginal applicator. The large majority of points on the transverse and coronal planes met the gamma index 5% and 2 mm pass rate criterion. Bannon *et al.* examined ^{103}Pd and ^{192}Ir sources using a 0.5 mm dose grid and a 2% and 2 mm criterion, and obtained passing rates of 99.6% and 99.9% for linear sources and 98.9% and 100% for toroidal sources, respectively.[194]

Based on this literature and observations made when creating the AAPM TG-43U1 report, a gamma index criterion of 2.0% and 2.0 mm with a ≥99% pass rate for clinically relevant points may generally be used to evaluate agreement of MBDCA-based TPS results with reference treatment plans. At the same time, setting tolerance levels is a major endeavor and the set of criteria for acceptability might need to be adjusted depending on the complexity of the case, such as in Venselaar *et al.*[195] Hence, more research, similar to the study by Stock *et al.* is needed to establish clear sets of criteria,[196] and further validation and cross comparison with MC and other MBDCAs should be a major area of research.

V.C.4. Phantom development

Finally, there is a need to design and implement relevant physical phantom geometries with known materials, possibly adding various applicator/shield inserts. For these phantoms, it is necessary to assess the dose distributions experimentally (e.g., using TLDs, radiochromic film, or GEL dosimeters) and compare the results with a virtual representation within a MBDCA TPS.[72] This process would generate sets of "true" independent reference data against which clinical medical physicists can validate their TPS and for which new systems can be benchmarked. Again, the proposed Registry would play a central role in this process.

VI. OTHER ISSUES AND LIMITATIONS

VI.A. Uncertainties related to MBDCA

There are several sources of MBDCA dosimetric uncertainties; many are common to all calculation methods. In this section, both general and method-specific dosimetric uncertainties are identified. A list of dosimetric uncertainty components in approximate chronological order is given in Table IV, and includes several items and expands upon those from the joint AAPM/ESTRO TG-138 report for direct MC simulations of brachytherapy source dosimetry.[197] While quantitative uncertainties are not recommended due to the paucity of the literature on this topic and the variability of results based on different possibilities of applicator/source/site, an indication of which items are generally guided by MBDCA design or the physicist is made available. Based on presently available choices within the TPS, responsibility for some of these components may fall to the medical physicist.

For all MBDCA approaches to brachytherapy treatment planning, Type B dosimetric uncertainties (nonstatistical or systematic) are present. Specific to MC methods, statistical, or Type A, uncertainties become more pronounced with limited particle histories, while Type B uncertainties may occur if certain variance reduction techniques are used, which introduce biases, such as the MC condensed-history algorithm for charged particle transport. Specific to GBBS

TABLE IV. Dosimetric uncertainties for MBDCA, with control over a given uncertainty component indicated by the responsible party.

#	Dosimetric uncertainty components	Responsible party
1	Source (seed) modeling such as geometry, material specifications, etc. For HDR and PDR ^{192}Ir sources, the length of cable modeled with the source also leads to uncertainties (Ref. 71). Also for HDR ^{192}Ir sources, often times virtual sources are used where such geometric approximations can lead to dosimetric uncertainties.	Vendor
2	Applicator modeling (if applicable) such as geometries, material specifications (especially denser materials such as lead or tungsten alloys).	Vendor
3	Source and applicator characterization grid size resolution if not explicitly modeled.	Physicist
4	Source and/or applicator positioning in the patient anatomy, which is extremely important for shadowing effects behind dense materials, such as additional seeds (if applicable), dense shielding materials, or light material streaming paths such as through catheters.	Physicist
5	Modeling of brachytherapy source radiation emissions.	Vendor
6	Patient geometry and limitations to simulate the realistic geometry.	Physicist
7	Material voxels grid resolution size (based on CT scanning).	Physicist
8	Determination of patient composition through correlation of CT HU to material and density mapping.	Vendor and physicist
9	Fundamental material interaction data used (cross sections).	Vendor
10	MBDCA model and potential simplifications away from realistic physics models.	Vendor
11	Use of collision kerma versus absorbed dose, especially in tissue areas where CPE assumption is not true (near interfaces of applicator and gas/tissue interface).	Vendor
12	Output voxel grid resolution size.	Physicist

methods, systematic uncertainties arise from spatial, angular, and energy discretization due to use of a finite grid. Specific to CC methods, systematic uncertainties arise from the use of angular discretization (i.e., collapsed point-spread kernels) combined with a finite grid.

MBDCAs using MC or GBBS methods are similar as both methods converge to the LBTE solution. Therefore, uncertainties for MC and GBBS can be reduced by increasing the number of particles or the resolution in space, angle, and energy, respectively. Based on point-kernel superposition,[9,10,16,57,58,198,199] the CC method involves no approximations up to and including the dose from once scattered photons. However, dose from multiply scattered photons calculated by CC involves an approximation related to phantom size from initial generation of point kernels for multiply scattered photons and use of rectilinear methods to scale the multiple-scatter kernel for material heterogeneities. Dosimetric uncertainties for MC, GBBS, and CC usually increase with increasing distance from the source and with decreasing voxel dimensions, and can be reduced at the expense of increased calculation time through use of more histories (MC) or denser grids (GBBS, CC).

In trying to limit some of these uncertainties, a calculation voxel size no larger than $(2\ \text{mm})^3$ should be used at all times. If allowed by the imaging data set resolution, smaller voxel sizes [$< (1\ \text{mm})^3$] could be used. This would be of particular interest in close proximity to sources and interfaces. Furthermore, dose uncertainties obtained using MC MBDCAs for the volume of interest (e.g., CTV, PTV, etc.) should be reported *systematically*. For the time being, the approach of Sec. III.D.1 of TG-105 (Ref. 85) is recommended, with a threshold of using voxels with dose values 25% or greater than the prescription dose. This change in threshold is needed since brachytherapy has steeper dose gradients than EBRT.

VI.B. Limitations

There may be certain limitations imposed by each of the MBDC engines as implemented in TPS software. Examples of such limitations include:

(1) Limits on which brachytherapy seeds are supported.
(2) Limits on the types of brachytherapy sources supported (i.e., HDR or PDR versus LDR).
(3) Limits on the applicators supported (if applicable).
(4) Limits on the materials (and associated compositions) that can be assigned.
(5) Nonchangeable CT HU to material and density conversions.
(6) Only dose reporting as $D_{m,m}$ or $D_{w,m}$ may be supported and not both.
(7) Upper and lower limits may be placed on the dose grid resolution size.
(8) Limits on the extent of the patient geometry may be imposed.
(9) User control over algorithm parameters may be limited.

Through coordination amongst clinical professional societies, TPS vendors, and source manufacturers, it is hoped that many of the current limitations will be overcome in the near future.

VI.C. Considerations for changing brachytherapy dose prescriptions

There is a long history in the field of brachytherapy of safely changing prescriptions based on dosimetric advancements. Source strength units have evolved from mg-Ra-eq to apparent activity to air-kerma strength, S_K and reference air-kerma rate, the currently accepted two measures of source strength for LE and HE photon-emitting brachytherapy sources.[200] These changes have primarily resulted in prescriptions using absorbed dose instead of specification in terms of source strength and implant duration. More recently, establishment of the AAPM TG-43 formalism and migration of the LE S_K standard to the NIST WAFAC has resulted in prescription dose changes of about −10% for LDR ^{125}I seeds, with permanent prostate implant prescriptions changing from 160 Gy to 145 Gy,[201] and COMS eye plaque application prescriptions from 100 Gy to 85 Gy.[202] Further, when accounting for COMS eye plaque material heterogeneities and radiation scatter conditions between $D_{w,w\text{-}TG43}$ and $D_{w,m}$, the prescribed dose of 85 Gy corresponds to an administered dose of 76 Gy for ^{125}I (−11%) and 67 Gy for ^{103}Pd (−21%) sources.[191] Such large dose changes are not expected for HE photon-emitting brachytherapy sources.

A dose tolerance of ±5% was adopted by the ABS for addressing dosimetric changes upon implementing dosimetry recommendations of the 2004 AAPM TG-43U1 report.[4,5,203,204] As more data become available on differences between prescribed and administered doses, the brachytherapy community will be better positioned to evaluate whether prescription changes are warranted for specific disease-sites.

Based on the significance of heterogeneity effects, the AAPM, ESTRO, ABS, and ABG recommend for those clinics that have the necessary resources that dose calculations be performed not only according to the TG-43 formalism, but also using the more accurate heterogeneous calculations. For the latter, the recommendations made in the previous sections should be followed closely. These dose estimates should be kept on file for a clinical evaluation in anticipation of sufficient heterogeneity-enabled brachytherapy TPS. While there remain significant dosimetric uncertainties and limitations as examined in Subsections VI.A and VI.B, the capabilities of MBDCAs to account for material heterogeneities, patient scatter conditions, and attenuation amongst sources and by high-Z applicators require the radiation oncologist to assess the clinical practice of brachytherapy using MBDCA-based dosimetry. Until sufficient clinical data become available to issue specific societal recommendations on dose prescriptions, the AAPM, ESTRO, ABS, and ABG recommend that prescriptions based on the TG-43 dose calculation formalism remain in effect. Similarly, for the time being MBDCAs are generally impractical (from a computational time

perspective) for dose optimization and the TG-43 formalism remains the standard of practice for this task.

VII. CONCLUSIONS

The AAPM TG-43 dose calculation formalism has provided the brachytherapy community with clear processes in terms of source strength specification and efficient dose calculations that made it easier to compare dose-outcome relationships among different institutions. For the time being, the TG-43 formalism will remain an important part of clinical brachytherapy. This report recognizes the benefit of the current standard and has built upon the developed infrastructure with specific recommendations to help move the brachytherapy field towards greater adoption of more accurate, advanced model-based dose calculation algorithms. Application of TG-186 guidance should help to ensure that the shared worldwide experience in using the TG-43 formalism is not lost in the process of seeking better brachytherapy dose calculation tools. The report also underlines specific research areas that brachytherapy physicists and physicians should tackle expeditiously, perhaps through consortium efforts to provide data required to move forward with MBDCAs.

Furthermore, it is important to acknowledge that the bulk of clinical brachytherapy dosimetry experience is with radiation transport and energy deposition in water, with dose to water reported (as calculated under the TG-43 approach). Hence, for the time being the recommendation that TG-43 calculations be performed in parallel with model-based dose calculations is crucial. Only in this way will the radiation therapy community become familiar with dose differences, including the impact on prescription dose and doses to points, organs, and regions of interest. This will enable assessment of the implications of adopting MBDCAs for treatment planning, and help the brachytherapy community to understand new study results and place them in the context of previous dose calculations, treatment planning, and research.

ACKNOWLEDGMENTS

The authors wish to acknowledge the contribution to comments and reviews by Dr. Annette Haworth on behalf of the Australasian Brachytherapy Group. The authors further acknowledge Dr. Jack Venselaar (liaison between GEC-ESTRO and AAPM-BTSC) and Dr. Frank-André Siebert (chair of BRAPHYQS) for pursuing the review effort within ESTRO. The final approval of this document by ESTRO would not have been possible without the support of Dr. Christine Haie-Meder (Chair of GEC-ESTRO) and Dr. Jean Bourhis (former President of ESTRO). Similarly, the authors acknowledge Mr. Zoubir Ouhib as chair of the ABS physics committee for seeking support of this report within the ABS. The authors finally wish to thank Dr. Facundo Ballester, Dr. Joseph Bucci, Dr. José Perez-Calatayud, Dr. Dean Cutajar, Dr. Martin Ebert, Dr. Moyed Miften, Dr. Jean Moran, Dr. Panagiottis Papagiannis, Dr. Niko Papanikolaou, Dr. Chet Reft, Dr. Theadore Robin, Jr., Dr. Ronald Sloboda, and Dr. Ning J. Yue for the careful review of this report.

APPENDIX A: GLOSSARY OF TERMS

AAPM	American Association of Physicists in Medicine
ABS	American Brachytherapy Society
ABG	Australasian Brachytherapy Group
BV	BrachyVision
BT	brachytherapy
CBCT	Cone beam computed tomography
CC	Collapsed cone
COMS	Collaborative Ocular Melanoma Study
CPE	Charged particle equilibrium
CSDA	Continuous slowing down approximation
CT	Computed tomography
DECT	Dual-energy CT
DICOM	Digital imaging and communications in medicine, the standard used for medical images and many other forms of digital data in radiotherapy
DICOM-RT	An extension of the DICOM standard that handles the radiotherapy modality
DVH	Dose-volume histogram
EBRT	External beam radiation therapy
EBS	Electronic brachytherapy source
ESTRO	European Society for Radiotherapy and Oncology
ESTRO-EIR	European Institute of Radiotherapy; A standing committee of ESTRO
GBBS	Grid-based Boltzmann equation solver, such as used by the Acuros® system
GEC-ESTRO	Groupe Européen de Curiethérapie; A standing committee of ESTRO; representing brachytherapy
GYN	Gynecological
HDR	High dose-rate
HU	Hounsfield unit
ICRU	International Commission on Radiation Units and Measurements
ICRP	International Commission on Radiological Protection
kV	Kilovoltage
LBTE	Linear Boltzmann transport equation
LDR	Low dose-rate
MC	Monte Carlo
MBDCA	Model-based dose calculation algorithm An algorithm that uses source models and details of the patient and applicator geometry to calculate a three-dimensional dose distribution in the patient as opposed to look-up tables based on a water geometry
MRI	Magnetic resonance imaging
MV	Megavoltage
NIST	National Institute of Standards and Technology
PDR	Pulsed dose rate
POI	Point of interest
Primary dose	Dose contributed by direct, nonscattered photons

QA	Quality assurance
QC	Quality control
ROI	Region of interest
RPC	Radiological Physics Center
Scatter dose	Dose contributed by scattered photons
Segmentation	When applied to tissues, the spatial delineation of different regions of a 3D image dataset and assignment of elemental compositions and mass (or electron) densities
TLD	Thermoluminescent dosimeter
TPS	Treatment planning system
TG	Task group
US	Ultrasound (imaging)
VBD	Volume breast density, defined as the fractional volume of glandular tissue
WAFAC	Wide-angle free-air chamber

[a]Author to whom correspondence should be addressed. Electronic mail: beaulieu@phy.ulaval.ca

[1]B. R. Thomadsen, J. F. Williamson, M. J. Rivard, and A. S. Meigooni, "Anniversary paper: Past and current issues, and trends in brachytherapy physics," Med. Phys. **35**, 4708–4723 (2008).
[2]B. S. Hilaris, U. K. Henschke, and J. G. Holt, "Clinical experience with long half-life and low-energy encapsulated radioactive sources in cancer radiation therapy," Radiology **91**, 1163–1167 (1968).
[3]R. Nath, L. L. Anderson, G. Luxton, K. A. Weaver, J. F. Williamson, and A. S. Meigooni, "Dosimetry of interstitial brachytherapy sources: Recommendations of the AAPM Radiation Therapy Committee Task Group No. 43," Med. Phys. **22**, 209–234 (1995).
[4]M. J. Rivard, B. M. Coursey, L. A. DeWerd, W. F. Hanson, M. S. Huq, G. S. Ibbott, M. G. Mitch, R. Nath, and J. F. Williamson, "Update of AAPM Task Group No. 43 Report: A revised AAPM protocol for brachytherapy dose calculations," Med. Phys. **31**, 633–674 (2004).
[5]M. J. Rivard, W. M. Butler, L. A. DeWerd, M. S. Huq, G. S. Ibbott, A. S. Meigooni, C. S. Melhus, M. G. Mitch, R. Nath, and J. F. Williamson, "Supplement to the 2004 update of the AAPM Task Group No. 43 Report," Med. Phys. **34**, 2187–2205 (2007).
[6]J. F. Williamson, "The Sievert integral revisited: Evaluation and extension to ^{125}I, ^{169}Yb, and ^{192}Ir brachytherapy sources," Int. J. Radiat. Oncol., Biol., Phys. **36**, 1239–1250 (1996).
[7]H. Meertens and R. van der Laarse, "Screens in ovoids of a Selectron cervix applicator," Radiother. Oncol. **3**, 69–80 (1985).
[8]K. J. Weeks and J. C. Dennett, "Dose calculation and measurements for a CT compatible version of the Fletcher applicator," Int. J. Radiat. Oncol., Biol., Phys. **18**, 1191–1198 (1990).
[9]Å. K. Carlsson and A. Ahnesjö, "The collapsed cone superposition algorithm applied to scatter dose calculations in brachytherapy," Med. Phys. **27**, 2320–2332 (2000).
[10]J. F. Williamson, R. S. Baker, and Z. Li, "A convolution algorithm for brachytherapy dose computations in heterogeneous geometries," Med. Phys. **18**, 1256–1265 (1991).
[11]J. F. Williamson, Z. Li, and J. W. Wong, "One-dimensional scatter-subtraction method for brachytherapy dose calculation near bounded heterogeneities," Med. Phys. **20**, 233–244 (1993).
[12]M. J. Rivard, J. L. M. Venselaar, and L. Beaulieu, "The evolution of brachytherapy treatment planning," Med. Phys. **36**, 2136–2153 (2009).
[13]N. Papanikolaou, J. J. Battista, A. L. Boyer, C. Kappas, E. Klein, T. R. Mackie, M. Sharpe, and J. Van Dyk, "AAPM Report No. 85: Tissue inhomogeneity corrections for megavoltage photon beams," *AAPM Report No. 85* (Medical Physics, Madison, WI, 2004), pp. 1–135.
[14]A. Ahnesjö and M. M. Aspradakis, "Dose calculations for external photon beams in radiotherapy," Phys. Med. Biol. **44**, R99–R155 (1999).
[15]A. Ahnesjö, "Collapsed cone convolution of radiant energy for photon dose calculation in heterogenous media," Med. Phys. **16**, 577–592 (1989).
[16]T. R. Mackie, J. W. Scrimger, and J. J. Battista, "A convolution method of calculating dose for 15-MV x rays," Med. Phys. **12**, 188–196 (1985).
[17]D. W. O. Rogers, "Fifty years of Monte Carlo simulations for medical physics," Phys. Med. Biol. **51**, R287–R301 (2006).
[18]K. A. Gifford, J. L. Horton, Jr., T. A. Wareing, G. Failla, and F. Mourtada, "Comparison of a finite-element multigroup discrete-ordinates code with Monte Carlo for radiotherapy calculations," Phys. Med. Biol. **51**, 2253–2265 (2006).
[19]O. N. Vassiliev, T. A. Wareing, J. McGhee, G. Failla, M. R. Salehpour, and F. Mourtada, "Validation of a new grid-based Boltzmann equation solver for dose calculation in radiotherapy with photon beams," Phys. Med. Biol. **55**, 581–598 (2010).
[20]International Commission on Radiation Units and Measurements, "Tissue substitutes in radiation dosimetry and measurement," ICRU Report No. 44 (ICRU Publications, Bethesda, MD, 1989).
[21]R. E. P. Taylor, "Monte Carlo calculations for brachytherapy," M.Sc. thesis, Carleton University, Ottawa, Canada, 2006.
[22]R. M. Thomson, R. E. P. Taylor, and D. W. O. Rogers, "Monte Carlo dosimetry for ^{125}I and ^{103}Pd eye plaque brachytherapy," Med. Phys. **35**, 5530–5543 (2008).
[23]O. Chibani, J. F. Williamson, and D. Todor, "Dosimetric effects of seed anisotropy and interseed attenuation for ^{103}Pd and ^{125}I prostate implants," Med. Phys. **32**, 2557–2566 (2005).
[24]J. F. Carrier, L. Beaulieu, F. Therriault-Proulx, and R. Roy, "Impact of interseed attenuation and tissue composition for permanent prostate implants," Med. Phys. **33**, 595–604 (2006).
[25]J. F. Carrier, M. D'Amours, F. Verhaegen, B. Reniers, A. G. Martin, E. Vigneault, and L. Beaulieu, "Postimplant dosimetry using a Monte Carlo dose calculation engine: A new clinical standard," Int. J. Radiat. Oncol., Biol., Phys. **68**, 1190–1198 (2007).
[26]Y. Yang and M. J. Rivard, "Evaluation of brachytherapy lung implant dose distributions from photon-emitting sources due to tissue heterogeneities," Med. Phys. **38**, 5857–5862 (2011).
[27]J. G. H. Sutherland, K. M. Furutani, Y. I. Garces, and R. M. Thomson, "Model-based dose calculations for ^{125}I lung brachytherapy," Med. Phys. **39**, 4365–4377 (2012).
[28]G. Lymperopoulou, P. Papagiannis, A. Angelopoulos, P. Karaiskos, E. Georgiou, and D. Baltas, "A dosimetric comparison of ^{169}Yb and ^{192}Ir for HDR brachytherapy of the breast, accounting for the effect of finite patient dimensions and tissue inhomogeneities," Med. Phys. **33**, 4583–4589 (2006).
[29]P. Papagiannis, P. Karaiskos, E. Georgiou, D. Baltas, G. Lymperopoulou, E. Pantelis, and L. Sakelliou, "On the use of high dose rate ^{192}Ir and ^{169}Yb sources with the Mammosite® radiation therapy system," Med. Phys. **34**, 3614–3619 (2007).
[30]G. Anagnostopoulos, D. Baltas, E. Pantelis, P. Papagiannis, and L. Sakelliou, "The effect of patient inhomogeneities in oesophageal ^{192}Ir HDR brachytherapy: A Monte Carlo and analytical dosimetry study," Phys. Med. Biol. **49**, 2675–2685 (2004).
[31]E. Poon, J. F. Williamson, T. Vuong, and F. Verhaegen, "Patient-specific Monte Carlo dose calculations for high-dose-rate endorectal brachytherapy with shielded intracavitary applicator," Int. J. Radiat. Oncol., Biol., Phys. **72**, 1259–1266 (2008).
[32]X. Yan, E. Poon, B. Reniers, T. Vuong, and F. Verhaegen, "Comparison of dose calculation algorithms for colorectal cancer brachytherapy treatment with a shielded applicator," Med. Phys. **35**, 4824–4830 (2008).
[33]E. Poon and F. Verhaegen, "Development of a scatter correction technique and its application to HDR ^{192}Ir multicatheter breast brachytherapy," Med. Phys. **36**, 3703–3713 (2009).
[34]G. X. Ding, D. M. Duggan, and C. W. Coffey, "Accurate patient dosimetry of kilovoltage cone-beam CT in radiation therapy," Med. Phys. **35**, 1135–1144 (2008).
[35]G. X. Ding and C. W. Coffey, "Radiation dose from kilovoltage cone beam computed tomography in an image-guided radiotherapy procedure," Int. J. Radiat. Oncol., Biol., Phys. **73**, 610–617 (2009).
[36]B. R. B. Walters, G. X. Ding, R. Kramer, and I. Kawrakow, "Skeletal dosimetry in cone beam computed tomography," Med. Phys. **36**, 2915–2922 (2009).
[37]J. F. Williamson, "Semiempirical dose-calculation models in brachytherapy," in *Brachytherapy Physics*, 2nd ed., edited by B. R. Thomadsen, M. J. Rivard, and W. M. Butler (Medical Physics, Madison, WI, 2005), pp. 201–232.

[38]J. F. Williamson and M. J. Rivard, "Quantitative dosimetry methods for brachytherapy," in *Brachytherapy Physics*, 2nd ed., edited by B. R. Thomadsen, M. J. Rivard, and W. M. Butler (Medical Physics, Madison, WI, 2005), pp. 233–294.
[39]Y. Yu, L. L. Anderson, Z. Li, D. E. Mellenberg, R. Nath, M. C. Schell, F. M. Waterman, A. Wu, and J. C. Blasko, "Permanent prostate seed implant brachytherapy: Report of the American Association of Physicists in Medicine Task Group No. 64," Med. Phys. **26**, 2054–2076 (1999).
[40]F. Ballester, D. Granero, J. Pérez-Calatayud, C. S. Melhus, and M. J. Rivard, "Evaluation of high-energy brachytherapy source electronic disequilibrium and dose from emitted electrons," Med. Phys. **36**, 4250–4256 (2009).
[41]C. C. Ling and E. D. Yorke, "Interface dosimetry for I-125 sources," Med. Phys. **16**, 376–381 (1989).
[42]E. D. Yorke, Y. C. D. Huang, M. C. Schell, R. Wong, and C. C. Ling, "Clinical implications of I-125 dosimetry of bone and bone-soft tissue interfaces," Int. J. Radiat. Oncol., Biol., Phys. **21**, 1613–1619 (1991).
[43]J. F. Williamson, "Dose calculations about shielded gynecological colpostats," Int. J. Radiat. Oncol., Biol., Phys. **19**, 167–178 (1990).
[44]R. Nath, C. H. Park, C. R. King, and P. Muench, "A dose computation model for ^{241}Am vaginal applicators including the source-to-source shielding effects," Med. Phys. **17**, 833–842 (1990).
[45]A. S. Kirov and J. F. Williamson, "Two-dimensional scatter integration method for brachytherapy dose calculations in 3D geometry," Phys. Med. Biol. **42**, 2119–2135 (1997).
[46]G. M. Daskalov, A. S. Kirov, and J. F. Williamson, "Analytical approach to heterogeneity correction factor calculation for brachytherapy," Med. Phys. **25**, 722–735 (1998).
[47]G. Anagnostopoulos, D. Baltas, P. Karaiskos, E. Pantelis, P. Papagiannis, and L. Sakelliou, "An analytical dosimetry model as a step towards accounting for inhomogeneities and bounded geometries in ^{192}Ir brachytherapy treatment planning," Phys. Med. Biol. **48**, 1625–1647 (2003).
[48]R. Wang and R. S. Sloboda, "Brachytherapy scatter dose calculation in heterogeneous media: I. A microbeam ray-tracing method for the single-scatter contribution," Phys. Med. Biol. **52**, 5619–5636 (2007).
[49]R. Wang and R. S. Sloboda, "Brachytherapy scatter dose calculation in heterogeneous media: II. Empirical formulation for the multiple-scatter contribution," Phys. Med. Biol. **52**, 5637–5654 (2007).
[50]C. Furstoss, B. Reniers, M. J. Bertrand, E. Poon, J. F. Carrier, B. M. Keller, J.-P. Pignol, L. Beaulieu, and F. Verhaegen, "Monte Carlo study of LDR seed dosimetry with an application in a clinical brachytherapy breast implant," Med. Phys. **36**, 1848–1858 (2009).
[51]J. Markman, J. F. Williamson, J. F. Dempsey, and D. A. Low, "On the validity of the superposition principle in dose calculations for intracavitary implants with shielded vaginal colpostats," Med. Phys. **28**, 147–155 (2001).
[52]M. D'Amours, J. Carrier, E. Lessard, J. Pouliot, F. Verhaegen, and L. Beaulieu, "A new approach for afterloading brachytherapy inverse planned dose optimization based on the accurate Monte Carlo method," Med. Phys. **35**, 2969 (2008) (abstract).
[53]M. D'Amours, J. Pouliot, A. Dagnault, F. Verhaegen, and L. Beaulieu, "Patient-specific Monte Carlo-based dose-kernel approach for inverse planning in afterloading brachytherapy," Int. J. Radiat. Oncol., Biol., Phys. **81**, 1582–1589 (2011).
[54]M. J. Rivard, C. S. Melhus, D. Granero, J. Perez-Calatayud, and F. Ballester, "An approach to using conventional brachytherapy software for clinical treatment planning of complex, Monte Carlo-based brachytherapy dose distributions," Med. Phys. **36**, 1968–1975 (2009).
[55]M. J. Price and F. Mourtada, "A 3D forward treatment planning algorithm using pre-calculated Monte Carlo data sets for HDR/PDR tandem and ovoid intracavitary systems," Brachytherapy **6**, S89 (2007) (abstract).
[56]Y. Yang, C. S. Melhus, S. Sioshansi, and M. J. Rivard, "Treatment planning of a skin-sparing conical breast brachytherapy applicator using conventional brachytherapy software," Med. Phys. **38**, 1519–1525 (2011).
[57]Å. K. Carlsson and A. Ahnesjö, "Point kernels and superposition methods for scatter dose calculations in brachytherapy," Phys. Med. Biol. **45**, 357–382 (2000).
[58]Å. K. Carlsson Tedgren and A. Ahnesjö, "Accounting for high *Z* shields in brachytherapy using collapsed cone superposition for scatter dose calculation," Med. Phys. **30**, 2206–2217 (2003).
[59]Å. K. Carlsson Tedgren and A. Ahnesjö, "Optimization of the computational efficiency of a 3D, collapsed cone dose calculation algorithm for brachytherapy," Med. Phys. **35**, 1611–1618 (2008).
[60]J. E. O'Connor, "The variation of scattered x-rays with density in an irradiated body," Phys. Med. Biol. **1**, 352–369 (1957).
[61]K. R. Russell, Å. K. Carlsson Tedgren, and A. Ahnesjö, "Brachytherapy source characterization for improved dose calculations using primary and scatter dose separation," Med. Phys. **32**, 2739–2752 (2005).
[62]B. van Veelen, "Collapsed cone dose calculations for model based brachytherapy utilizing Monte Carlo source characterization data," in *Proceedings of the International Workshop on Recent Advances in Monte Carlo techniques for radiation therapy*, McGill University, Montreal, Quebec, Canada (2011), available at http://www.medphys.mcgill.ca/~ws2011/Abstract_book.html.
[63]E. E. Lewis and W. F. Miller, *Computational Methods of Neutron Transport* (Wiley, New York, 1984).
[64]C. Zhou and F. Inanc, "Integral-transport-based deterministic brachytherapy dose calculations," Phys. Med. Biol. **48**, 73–93 (2003).
[65]R. E. Alcouffe, R. S. Baker, F. W. Brinkley, D. R. Marr, R. D. O'Dell, and W. F. Walters, "DANTSYS: a diffusion accelerated neutral particle transport code system," Los Alamos National Laboratory Report No. LA-12969-M, Los Alamos, NM, 1995.
[66]G. M. Daskalov, R. S. Baker, D. W. O Rogers, and J. F. Williamson, "Dosimetric modeling of the microselectron high-dose rate ^{192}Ir source by the multigroup discrete ordinates method," Med. Phys. **27**, 2307–2319 (2000).
[67]G. M. Daskalov, R. S. Baker, D. W. O. Rogers, and J. F. Williamson, "Multigroup discrete ordinates modeling of ^{125}I 6702 seed dose distributions using a broad energy-group cross section representation," Med. Phys. **29**, 113–124 (2002).
[68]F. Mourtada, T. Wareing, J. L. Horton, Jr., J. McGhee, D. Barnett, K. Gifford, G. Failla, and R. Mohan, "A deterministic dose calculation method applied to the dosimetry of shielded intracavitary brachytherapy applicators," Med. Phys. **31**, 1807–1808 (2004) (abstract).
[69]K. A. Gifford, M. J. Price, J. L. Horton, Jr., T. A. Wareing, and F. Mourtada, "Optimization of deterministic transport parameters for the calculation of the dose distribution around a high dose-rate ^{192}Ir brachytherapy source," Med. Phys. **35**, 2279–2285 (2008).
[70]K. Zourari, E. Pantelis, A. Moutsatsos, L. Petrokokkinos, P. Karaiskos, L. Sakelliou, E. Georgiou, and P. Papagiannis, "Dosimetric accuracy of a deterministic radiation transport based ^{192}Ir brachytherapy treatment planning system. Part I: Single sources and bounded homogeneous geometries," Med. Phys. **37**, 649–661 (2010).
[71]J. K. Mikell and F. Mourtada, "Dosimetric impact of an ^{192}Ir brachytherapy source cable length modeled using a grid-based Boltzmann transport equation solver," Med. Phys. **37**, 4733–4743 (2010).
[72]L. Petrokokkinos, K. Zourari, E. Pantelis, A. Moutsatsos, P. Karaiskos, L. Sakelliou, I. Seimenis, E. Georgiou, and P. Papagiannis, "Dosimetric accuracy of a deterministic radiation transport based ^{192}Ir brachytherapy treatment planning system. Part II: Monte Carlo and experimental verification of a multiple source dwell position plan employing a shielded applicator," Med. Phys. **38**, 1981–1992 (2011).
[73]K. Bush, I. M. Gagne, S. Zavgorodni, W. Ansbacher, and W. Beckham, "Dosimetric validation of Acuros® XB with Monte Carlo methods for photon dose calculations," Med. Phys. **38**, 2208–2221 (2011).
[74]T. Han, J. K. Mikell, M. Salehpour, and F. Mourtada, "Dosimetric comparison of Acuros XB deterministic radiation transport method with Monte Carlo and model-based convolution methods in heterogeneous media," Med. Phys. **38**, 2651–2664 (2011).
[75]A. Fogliata, G. Nicolini, A. Clivio, E. Vanetti, P. Mancosu, and L. Cozzi, "Dosimetric validation of the Acuros XB advanced dose calculation algorithm: Fundamental characterization in water," Phys. Med. Biol. **56**, 1879–1904 (2011).
[76]J. F. Williamson, "Monte Carlo evaluation of kerma at a point for photon transport problems," Med. Phys. **14**, 567–576 (1987).
[77]J. F. Williamson and M. J. Rivard, "Thermoluminescent detector and Monte Carlo techniques for reference-quality brachytherapy dosimetry," in *Clinical Dosimetry Measurements in Radiotherapy*, edited by D. W. O. Rogers and J. E. Cygler (Medical Physics, Madison, WI, 2009), pp. 437–499.
[78]H. Hedtjärn, G. Alm Carlsson, and J. F. Williamson, "Accelerated Monte Carlo based dose calculations for brachytherapy planning using correlated sampling," Phys. Med. Biol. **47**, 351–376 (2002).
[79]A. Sampson, Y. Le, D. Todor, and J. F. Williamson, "Using correlated sampling to accelerate CT-based Monte Carlo dose calculations for brachytherapy treatment planning," in *Proceedings from the World*

Congress on Medical Physics and Biomedical Engineering (11th International Congress of the IUPESM), Munich, Germany, edited by O. Dössel and W. C. Schlegel (Springer, Chennai, India, 2009), Vol. 25, pp. 311–314.
[80]O. Chibani and J. F. Williamson, "MCPI©: A sub-minute Monte Carlo dose calculation engine for prostate implants," Med. Phys. **32**, 3688–3698 (2005).
[81]R. E. P. Taylor, G. Yegin, and D. W. O. Rogers, "Benchmarking BrachyDose: Voxel based EGSnrc Monte Carlo calculations of TG-43 dosimetry parameters," Med. Phys. **34**, 445–457 (2007).
[82]R. M. Thomson, G. Yegin, R. E. P. Taylor, J. G. H. Sutherland, and D. W. O. Rogers, "Fast Monte Carlo dose calculations for brachytherapy with BrachyDose," Med. Phys. **37**, 3910 (2010) (abstract).
[83]H. H. Liu, "D_m rather than D_w should be used in Monte Carlo treatment planning: For the proposition," Med. Phys. **29**, 922–923 (2002).
[84]P. Keall, "D_m rather than D_w should be used in Monte Carlo treatment planning: Against the proposition," Med. Phys. **29**, 923–924 (2002).
[85]I. J. Chetty, B. Curran, J. E. Cygler, J. J. DeMarco, G. Ezzell, B. A. Faddegon, I. Kawrakow, P. J. Keall, H. Liu, C.-M. C. Ma, D. W. O. Rogers, J. Seuntjens, D. Sheikh-Bagheri, and J. V. Siebers, "Report of the AAPM Task Group No. 105: Issues associated with clinical implementation of Monte Carlo-based photon and electron external beam treatment planning," Med. Phys. **34**, 4818–4853 (2007).
[86]V. Gregoire, T. R. Mackie, W. De Neve, M. Gospodarowicz, J. A. Purdy, M. van Herk, A. Niemierko, A. Ahnesjö, M. Goitein, N. Gupta, and T. Landberg, "ICRU Report 83: Prescribing, recording, and reporting photon-beam intensity-modulated radiation therapy (IMRT)," J. ICRU **10**, 1–106 (2010).
[87]C.-M. Ma and J. Li, "Dose specification for radiation therapy: Dose to water or dose to medium?," Phys. Med. Biol. **56**, 3073–3089 (2011).
[88]B. R. B. Walters, R. Kramer, and I. Kawrakow, "Dose to medium versus dose to water as an estimator of dose to sensitive skeletal tissue," Phys. Med. Biol. **55**, 4535–4546 (2010).
[89]J. V. Siebers, P. J. Keall, A. E. Nahum, and R. Mohan, "Converting absorbed dose to medium to absorbed dose to water for Monte Carlo based photon beam dose calculations," Phys. Med. Biol. **45**, 983–995 (2000).
[90]J. V. Siebers, P. J. Keall, A. E. Nahum, and R. Mohan, "Reply to: 'Comments on "Converting absorbed dose to medium to absorbed dose to water for Monte Carlo based photon beam dose calculations"'," Med. Phys. **45**, L18–L19 (2000).
[91]M. Fippel and F. Nüsslin, "Comments on 'Converting absorbed dose to medium to absorbed dose to water for Monte Carlo based photon beam dose calculations'," Phys. Med. Biol. **45**, L17–L18 (2000).
[92]N. Dogan, J. V. Siebers, and P. Keall, "Clinical comparison of head and neck and prostate IMRT plans using absorbed dose to medium and absorbed dose to water," Med. Phys. **51**, 4967–4980 (2006).
[93]H. Paganetti, "Dose to water versus dose to medium in proton beam therapy," Phys. Med. Biol. **54**, 4399–4421 (2009).
[94]M. J. Berger, J. S. Coursey, M. A. Zucker, and J. Chang, ESTAR, PSTAR, and ASTAR: Computer programs for calculating stopping-power and range tables for electrons, protons, and helium ions (version 1.2.3, online), National Institute of Standards and Technology, Gaithersburg, MD, 2005 (available URL: http://physics.nist.gov/Star).
[95]E. J. Hall and A. J. Giaccia, *Radiobiology for the Radiologist*, 7th ed. (Lippincott, Philadelphia, PA, 2012).
[96]R. M. Thomson, A. Carlsson Tedgren, and J. Williamson, "Comparison of bulk medium dose descriptors and cellular absorbed doses for brachytherapy," in *Proceedings of the International Workshop on Recent Advances in Monte Carlo techniques for radiation therapy*, McGill University, Quebec, Canada, (2011), available at http://www.medphys.mcgill.ca/~ws2011/Abstract_book.html.
[97]S. A. Enger, A. Ahnesjö, F. Verhaegen, and L. Beaulieu, "Dose to tissue medium or water cavities as surrogate for the dose to cell nuclei at brachytherapy photon energies," Phys. Med. Biol. **57**, 4489–4500 (2012).
[98]G. Landry, B. Reniers, J.-P. Pignol, L. Beaulieu, and F. Verhaegen, "The difference of scoring dose to water or tissues in Monte Carlo dose calculations for low energy brachytherapy photon sources," Med. Phys. **38**, 1526–1533 (2011).
[99]M. J. Rivard, L. Beaulieu, and F. Mourtada, "Enhancements to commissioning techniques and quality assurance of brachytherapy treatment planning systems that use model-based dose calculation algorithms," Med. Phys. **37**, 2645–2658 (2010).
[100]A. Sampson, Y. Le, and J. F. Williamson, "Fast patient-specific Monte Carlo brachytherapy dose calculations via the correlated sampling variance reduction technique," Med. Phys. **39**, 1058–1068 (2012).
[101]I. Kawrakow, E. Mainegra-HIng, D. W. O. Rogers, F. Tessier, and B. R. B. Walters, "The EGSnrc code system: Monte Carlo simulation of photon and electron transport," Technical Report No. PIRS-701 (National Research Council Canada, Ottawa, ON, 2011) (available URL: http://irs.inms.nrc.ca/software/egsnrc/documentation/pirs701/).
[102]P. R. Almond and H. Svensson, "Ionization chamber dosimetry for photon and electron beams. Theoretical considerations," Acta Radiol. Ther. Phys. Biol. **16**, 177–186 (1977).
[103]F. H. Attix, *Introduction to Radiological Physics and Radiation Dosimetry* (Wiley, New York, 1986).
[104]E. Poon and F. Verhaegen, "A CT-based analytical dose calculation method for HDR ^{192}Ir brachytherapy," Med. Phys. **36**, 3982–3994 (2009).
[105]D. Y. C. Huang, M. C. Schell, K. A. Weaver, and C. C. Ling, "Dose distribution of ^{125}I sources in different tissues," Med. Phys. **17**, 826–832 (1990).
[106]A. S. Meigooni and R. Nath, "Tissue inhomogeneity correction for brachytherapy sources in a heterogeneous phantom with cylindrical symmetry," Med. Phys. **19**, 401–407 (1992).
[107]B. Reniers, F. Verhaegen, and S. Vynckier, "The radial dose function of low-energy brachytherapy seeds in different solid phantoms: Comparison between calculations with the EGSnrc and MCNP4C Monte Carlo codes and measurements," Phys. Med. Biol. **49**, 1569–1582 (2004).
[108]J. F. Williamson, S. Li, S. Devic, B. R. Whiting, and F. A. Lerma, "On two-parameter models of photon cross sections: Application to dual-energy CT imaging," Med. Phys. **33**, 4115–4129 (2006).
[109]International Commission on Radiation Units and Measurements, "Photon, electron, proton and neutron interaction data for body tissues," Report No. 46 (ICRU Publications, Bethesda, MD, 1992).
[110]H. Q. Woodard and D. R. White, "The composition of body tissues," Br. J. Radiol. **59**, 1209–1218 (1986).
[111]M. J. Yaffe, J. M. Boone, N. Packard, O. Alonzo-Proulx, S.-Y. Huang, C. L. Peressotti, A. Al-Mayah, and K. Brock, "The myth of the 50-50 breast," Med. Phys. **36**, 5437–5443 (2009).
[112]J. H. Suh, J. M. Gardner, K. H. Kee, S. Shen, A. G. Ayala, and J. Y. Ro, "Calcifications in prostate and ejaculatory system: A study on 298 consecutive whole mount sections of prostate from radical prostatectomy or cystoprostatectomy specimens," Ann. Diagn. Pathol. **12**, 165–170 (2008).
[113]B. Kassas, F. Mourtada, J. L. Horton, Jr., and R. G. Lane, "Contrast effects on dosimetry of a partial breast irradiation system," Med. Phys. **31**, 1976–1979 (2004).
[114]K. J. Weeks, "Monte Carlo dose calculations for a new ovoid shield system for carcinoma of the uterine cervix," Med. Phys. **25**, 2288–2292 (1998).
[115]M. J. Price, E. F. Jackson, K. A. Gifford, P. J. Eifel, and F. Mourtada, "Development of prototype shielded cervical intracavitary brachytherapy applicators compatible with CT and MR imaging," Med. Phys. **36**, 5515–5524 (2009).
[116]M. J. Price, J. L. Horton, K. A. Gifford, P. J. Eifel, A. Jhingran, A. A. Lawyer, P. A. Berner, and F. Mourtada, "Dosimetric evaluation of the Fletcher-Williamson ovoid for pulsed-dose-rate brachytherapy: A Monte Carlo study," Phys. Med. Biol. **50**, 5075–5087 (2005).
[117]G. Leclerc, M.-C. Lavallée, R. Roy, E. Vigneault, and L. Beaulieu, "Prostatic edema in ^{125}I permanent prostate implants: Dynamical dosimetry taking volume changes into account," Med. Phys. **33**, 574–583 (2006).
[118]G. Landry, B. Reniers, L. Murrer, L. Lutgens, E. Bloemen-Van Gurp, J.-P. Pignol, B. Keller, L. Beaulieu, and F. Verhaegen, "Sensitivity of low energy brachytherapy Monte Carlo dose calculations to uncertainties in human tissue composition," Med. Phys. **37**, 5188–5198 (2010).
[119]International Commission on Radiological Protection, "Report on the Task Group on Reference Man," ICRP Publication No. 23 (Pergamon, Oxford, 1975).
[120]International Commission on Radiological Protection, "Basic anatomical and physiological data for use in radiological protection: Reference values," ICRP Publication No. 89 (Pergamon, Oxford, 2002).
[121]M. Desbiens, M. D'Amours, H. Afsharpour, I. Thibault, E. Vigneault, and L. Beaulieu, "Monte Carlo dosimetry of high dose rate gynecologic interstitial brachytherapy," in *Proceedings of the International Workshop on Recent Advances in Monte Carlo techniques for radiation therapy*,

McGill, Quebec, Canada (2011), available at http://www.medphys.mcgill.ca/~ws2011/Abstract_book.html.
[122]J. K. Mikell, A. H. Klopp, G. M. N. Gonzalez, K. D. Kisling, M. J. Price, P. A. Berner, P. J. Eifel, and F. Mourtada, "Impact of heterogeneity-based dose calculation using a deterministic grid-based Boltzmann equation solver for intracavitary brachytherapy," Int. J. Radiat. Oncol., Biol., Phys. **83**, e417–e422 (2012).
[123]W. Kilby, J. Sage, and V. Rabett, "Tolerance levels for quality assurance of electron density values generated from CT in radiotherapy treatment planning," Phys. Med. Biol. **47**, 1485–1492 (2002).
[124]S. J. Thomas, "Relative electron density calibration of CT scanners for radiotherapy treatment planning," Br. J. Radiol. **72**, 781–786 (1999).
[125]B. Schaffner and E. Pedroni, "The precision of proton range calculations in proton radiotherapy treatment planning: Experimental verification of the relation between CT-HU and proton stopping power," Phys. Med. Biol. **43**, 1579–1592 (1998).
[126]U. Schneider, E. Pedroni, and A. Lomax, "The calibration of CT Hounsfield units for radiotherapy treatment planning," Phys. Med. Biol. **41**, 111–124 (1996).
[127]F. Verhaegen and S. Devic, "Sensitivity study for CT image use in Monte Carlo treatment planning," Phys. Med. Biol. **50**, 937–946 (2005).
[128]W. Schneider, T. Bortfeld, and W. Schlegel, "Correlation between CT numbers and tissue parameters needed for Monte Carlo simulations of clinical dose distributions," Phys. Med. Biol. **45**, 459–478 (2000).
[129]F. C. P. du Plessis, C. A. Willemse, M. G. Lötter, and L. Goedhals, "The indirect use of CT numbers to establish material properties needed for Monte Carlo calculation of dose distributions in patients," Med. Phys. **25**, 1195–1201 (1998).
[130]N. Kanematsu, N. Matsufuji, R. Kohno, S. Minohara, and T. Kanai, "A CT calibration method based on the polybinary tissue model for radiotherapy treatment planning," Phys. Med. Biol. **48**, 1053–1064 (2003).
[131]B. Vanderstraeten, P. W. Chin, M. Fix, A. Leal, G. Mora, N. Reynaert, J. Seco, M. Soukup, E. Spezi, W. De Neve, and H. Thierens, "Conversion of CT numbers into tissue parameters for Monte Carlo dose calculations: A multi-centre study," Phys. Med. Biol. **52**, 539–562 (2007).
[132]Y. Watanabe, "Derivation of linear attenuation coefficients from CT numbers for low-energy photons," Phys. Med. Biol. **44**, 2201–2211 (1999).
[133]R. A. Rutherford, B. R. Pullan, and I. Isherwood, "Measurement of effective atomic number and electron density using an EMI scanner," Neuroradiology **11**, 15–21 (1976).
[134]F. A. Dilmanian, X. Y. Wu, E. C. Parsons, B. Ren, J. Kress, T. M. Button, L. D. Chapman, J. A. Coderre, F. Giron, D. Greenberg, D. J. Krus, Z. Liang, S. Marcovici, M. J. Petersen, C. T. Roque, M. Shleifer, D. N. Slatkin, W. C. Thomlinson, K. Yamamoto, and Z. Zhong, "Single- and dual-energy CT with monochromatic synchrotron x-rays," Phys. Med. Biol. **42**, 371–387 (1997).
[135]B. J. Kirby, J. R. Davis, J. A. Grant, and M. J. Morgan, "Extracting material parameters from x-ray attenuation: A CT feasibility study using kilovoltage synchrotron x-rays incident upon low atomic number absorbers," Phys. Med. Biol. **48**, 3389–3409 (2003).
[136]E. D. Yorke, P. Keall, and F. Verhaegen, "Anniversary paper: Role of medical physicists and the AAPM in improving geometric aspects of treatment accuracy and precision," Med. Phys. **35**, 828–839 (2008).
[137]C. J. Moore, A. Amer, T. Marchant, J. R. Sykes, J. Davies, J. Stratford, C. McCarthy, C. MacBain, A. Henry, P. Price, and P. C. Williams, "Developments in and experience of kilovoltage x-ray cone beam image-guided radiotherapy," Br. J. Radiol. **79**, S66–S78 (2006).
[138]J. Hatton, B. McCurdy, and P. B. Greer, "Cone beam computerized tomography: The effect of calibration of the Hounsfield unit number to electron density on dose calculation accuracy for adaptive radiation therapy," Phys. Med. Biol. **54**, N329–N346 (2009).
[139]J. H. Siewerdsen and D. A. Jaffray, "Cone-beam computed tomography with a flat-panel imager: Magnitude and effects of x-ray scatter," Med. Phys. **28**, 220–231 (2001).
[140]Y. Yang, E. Schreibmann, T. Li, C. Wang, and L. Xing, "Evaluation of on-board kV cone beam CT (CBCT)-based dose calculation," Phys. Med. Biol. **52**, 685–705 (2007).
[141]B. Reniers and F. Verhaegen, "3D image-guided brachytherapy using cone beam CT," Brachytherapy **7**, 155–156 (2008) (abstract).
[142]H. Al-Halabi, L. Portelance, M. Duclos, B. Reniers, B. Bahoric, and L. Souhami, "Cone beam CT-based three-dimensional planning in high-dose-rate brachytherapy for cervical cancer," Int. J. Radiat. Oncol., Biol., Phys. **77**, 1092–1097 (2010).
[143]R. E. Alvarez and A. Macovski, "Energy-selective reconstructions in x-ray computerized tomography," Phys. Med. Biol. **21**, 733–744 (1976).
[144]J. Giersch, D. Niederlöhner, and G. Anton, "The influence of energy weighting on x-ray imaging quality," Nucl. Instrum. Methods Phys. Res. A **531**, 68–74 (2004).
[145]P. V. Granton, S. I. Pollmann, N. L. Ford, M. Drangova, and D. W. Holdsworth, "Implementation of dual- and triple-energy cone-beam micro-CT for postreconstruction material decomposition," Med. Phys. **35**, 5030–5042 (2008).
[146]J. P. Schlomka, E. Roessl, R. Dorscheid, S. Dill, G. Martens, T. Istel, C. Bäumer, C. Herrmann, R. Steadman, G. Zeitler, A. Livne, and R. Proksa, "Experimental feasibility of multi-energy photon-counting K-edge imaging in pre-clinical computed tomography," Phys. Med. Biol. **53**, 4031–4047 (2008).
[147]J. F. Sutcliffe, "A review of *in vivo* experimental methods to determine the composition of the human body," Phys. Med. Biol. **41**, 791–833 (1996).
[148]T. Xu, J. L. Ducote, J. T. Wong, and S. Molloi, "Feasibility of real time dual-energy imaging based on a flat panel detector for coronary artery calcium quantification," Med. Phys. **33**, 1612–1622 (2006).
[149]A. Laidevant, S. Malkov, C. I. Flowers, K. Kerlikowske, and J. A. Shepherd, "Compositional breast imaging using a dual-energy mammography protocol," Med. Phys. **37**, 164–174 (2010).
[150]B. J. Heismann, J. Leppert, and K. Stierstorfer, "Density and atomic number measurements with spectral x-ray attenuation method," J. Appl. Phys. **94**, 2073–2079 (2003).
[151]C. Rizescu, C. Beşliu, and A. Jipa, "Determination of local density and effective atomic number by the dual-energy computerized tomography method with the ^{192}Ir radioisotope," Nucl. Instrum. Methods Phys. Res. A **465**, 584–599 (2001).
[152]W. A. Kalender, W. H. Perman, J. R. Vetter, and E. Klotz, "Evaluation of a prototype dual-energy computed tomographic apparatus. I. Phantom studies," Med. Phys. **13**, 334–339 (1986).
[153]M. Bazalova, J. F. Carrier, L. Beaulieu, and F. Verhaegen, "Dual-energy CT-based material extraction for tissue segmentation in Monte Carlo dose calculations," Phys. Med. Biol. **53**, 2439–2456 (2008).
[154]G. Landry, B. Reniers, P. V. Granton, B. van Rooijen, L. Beaulieu, J. E. Wildberger, and F. Verhaegen, "Extracting atomic numbers and electron densities from a dual source dual energy CT scanner: Experiments and a simulation model," Radiother. Oncol. **100**, 375–379 (2011).
[155]G. Landry, P. V. Granton, B. Reniers, M. C. Öllers, L. Beaulieu, J. E. Wildberger, and F. Verhaegen, "Simulation study on potential accuracy gains from dual energy CT tissue segmentation for low-energy brachytherapy Monte Carlo dose calculations," Phys. Med. Biol. **56**, 6257–6278 (2011).
[156]T. Pawlicki and C.-M. Ma, "Effect of CT streaking artifacts in Monte Carlo dose distributions for head and neck cancer," in *The Use of Computers in Radiation Therapy: XIIIth International Conference*, edited by W. Schlegel and T. Bortfeld (Springer-Verlag, Heidelberg, 2000), pp. 414–416.
[157]W. A. Kalender, R. Hebel, and J. Ebersberger, "Reduction of CT artifacts caused by metallic implants," Radiology **164**, 576–577 (1987).
[158]J. C. Roeske, C. Lund, C. A. Pelizzari, X. Pan, and A. J. Mundt, "Reduction of computed tomography metal artifacts due to the Fletcher-Suit applicator in gynecology patients receiving intracavitary brachytherapy," Brachytherapy **2**, 207–214 (2003).
[159]M. Yazdi, L. Gingras, and L. Beaulieu, "An adaptive approach to metal artifact reduction in helical computed tomography for radiation therapy treatment planning: Experimental and clinical studies," Int. J. Radiat. Oncol., Biol., Phys. **62**, 1224–1231 (2005).
[160]J. Hsieh, "Adaptive streak artifact reduction in computed tomography resulting from excessive x-ray photon noise," Med. Phys. **25**, 2139–2147 (1998).
[161]B. De Man, J. Nuyts, P. Dupont, G. Marchal, and P. Suetens, "An iterative maximum-likelihood polychromatic algorithm for CT," IEEE Trans. Med. Imaging **20**, 999–1008 (2001).
[162]P. J. Keall, L. B. Chock, R. Jeraj, J. V. Siebers, and R. Mohan, "Image reconstruction and the effect on dose calculation for hip prostheses," Med. Dosim. **28**, 113–117 (2003).
[163]D. Xia, J. C. Roeske, L. Yu, C. A. Pelizzari, A. J. Mundt, and X. Pan, "A hybrid approach to reducing computed tomography metal artifacts in intracavitary brachytherapy," Brachytherapy **4**, 18–23 (2005).
[164]R. Murphy, D. L. Snyder, B. R. Whiting, D. G. Politte, and J. F. Williamson, "Incorporating known information into image

reconstruction algorithms for transmission tomography," Proc. SPIE **4684**, 29–37 (2002).
[165]J. F. Williamson, B. R. Whiting, J. Benac, R. J. Murphy, G. J. Blaine, J. A. O'Sullivan, D. G. Politte, and D. L. Snyder, "Prospects for quantitative computed tomography imaging in the presence of foreign metal bodies using statistical image reconstruction," Med. Phys. **29**, 2404–2418 (2002).
[166]M. Bazalova, L. Beaulieu, S. Palefsky, and F. Verhaegen, "Correction of CT artifacts and its influence on Monte Carlo dose calculations," Med. Phys. **34**, 2119–2132 (2007).
[167]C. Xu, F. Verhaegen, D. Laurendeau, S. A. Enger, and L. Beaulieu, "An algorithm for efficient metal artifact reductions in permanent seed implants," Med. Phys. **38**, 47–56 (2011).
[168]P. S. Basran, A. Robertson, and D. Wells, "CT image artifacts from brachytherapy seed implants: A postprocessing 3D adaptive median filter," Med. Phys. **38**, 712–718 (2011).
[169]A. K. H. Robertson, P. S. Basran, S. D. Thomas, and D. Wells, "CT, MR, and ultrasound image artifacts from prostate brachytherapy seed implants: The impact of seed size," Med. Phys. **39**, 2061–2068 (2012).
[170]C. Ménard, R. C. Susil, P. Choyke, G. S. Gustafson, W. Kammerer, H. Ning, R. W. Miller, K. L. Ullman, N. Sears Crouse, S. Smith, E. Lessard, J. Pouliot, V. Wright, E. McVeigh, C. N. Coleman, and K. Camphausen, "MRI-guided HDR prostate brachytherapy in standard 1.5T scanner," Int. J. Radiat. Oncol., Biol., Phys. **59**, 1414–1423 (2004).
[171]C. Haie-Meder, R. Pötter, E. Van Limbergen, E. Briot, M. De Brabandere, J. Dimopoulos, I. Dumas, T. P. Hellebust, C. Kirisits, S. Lang, S. Muschitz, J. Nevinson, A. Nulens, P. Petrow, and N. Wachter-Gerstner, "Recommendations from gynaecological (GYN) GEC-ESTRO Working Group (I): Concepts and terms in 3D image based 3D treatment planning in cervix cancer brachytherapy with emphasis on MRI assessment of GTV and CTV," Radiother. Oncol. **74**, 235–245 (2005).
[172]R. C. Krempien, S. Daeuber, F. W. Hensley, M. Wannenmacher, and W. Harms, "Image fusion of CT and MRI data enables improved target volume definition in 3D-brachytherapy treatment planning," Brachytherapy **2**, 164–171 (2003).
[173]M.-S. Chew, J. Xue, C. Houser, V. Misic, J. Cao, T. Cornwell, J. Handler, Y. Yu, and E. Gressen, "Impact of transrectal ultrasound- and computed tomography-based seed localization on postimplant dosimetry in prostate brachytherapy," Brachytherapy **8**, 255–264 (2009).
[174]G. Fichtinger, E. C. Burdette, A. Tanacs, A. Patriciu, D. Mazilu, L. L. Whitcomb, and D. Stoianovici, "Robotically assisted prostate brachytherapy with transrectal ultrasound guidance—Phantom experiments," Brachytherapy **5**, 14–26 (2006).
[175]I. B. Tutar, L. Gong, S. Narayanan, S. D. Pathak, P. S. Cho, K. Wallner, and Y. Kim, "Seed-based transrectal ultrasound-fluoroscopy registration method for intraoperative dosimetry analysis of prostate brachytherapy," Med. Phys. **35**, 840–848 (2008).
[176]J. Boda-Heggemann, F. M. Köhler, B. Küpper, D. Wolff, H. Wertz, S. Mai, J. Hesser, F. Lohr, and F. Wenz, "Accuracy of ultrasound-based (BAT) prostate-repositioning: A three-dimensional on-line fiducial-based assessment with cone-beam computed tomography," Int. J. Radiat. Oncol., Biol., Phys. **70**, 1247–1255 (2008).
[177]D. Fraser, Y. Chen, E. Poon, F. L. Cury, T. Falco, and F. Verhaegen, "Dosimetric consequences of misalignment and realignment in prostate 3DCRT using intramodality ultrasound image guidance," Med. Phys. **37**, 2787–2795 (2010).
[178]M. Krix, C. Plathow, M. Essig, K. Herfarth, J. Debus, H.-U. Kauczor, and S. Delorme, "Monitoring of liver metastases after stereotactic radiotherapy using low-MI contrast-enhanced ultrasound—Initial results," Eur. Radiol. **15**, 677–684 (2005).
[179]J. Zhou, P. Zhang, K. S. Osterman, S. A. Woodhouse, P. B. Schiff, E. J. Yoshida, Z. F. Lu, E. R. Pile-Spellman, G. J. Kutcher, and T. Liu, "Implementation and validation of an ultrasonic tissue characterization technique for quantitative assessment of normal-tissue toxicity in radiation therapy," Med. Phys. **36**, 1643–1650 (2009).
[180]J. G. H. Sutherland, R. M. Thomson, and D. W. O. Rogers, "Changes in dose with segmentation of breast tissues in Monte Carlo calculations for low-energy brachytherapy," Med. Phys. **38**, 4858–4865 (2011).
[181]H. Afsharpour, G. Landry, B. Reniers, J.-P. Pignol, L. Beaulieu, and F. Verhaegen, "Tissue modeling schemes in low energy breast brachytherapy," Phys. Med. Biol. **56**, 7045–7060 (2011).
[182]M. J. Rivard, "Monte Carlo calculations of AAPM Task Group Report No. 43 dosimetry parameters for the MED3631-A/M ^{125}I source," Med. Phys. **28**, 629–637 (2001).
[183]J. F. Williamson, "Dosimetric characteristics of the DRAXIMAGE model LS-1 I-125 interstitial brachytherapy source design: A Monte Carlo investigation," Med. Phys. **29**, 509–521 (2002).
[184]S.-Y. Huang, J. M. Boone, K. Yang, N. J. Packard, S. E. McKenney, N. D. Prionas, K. K. Lindfors, and M. J. Yaffe, "The characterization of breast anatomical metrics using dedicated breast CT," Med. Phys. **38**, 2180–2191 (2011).
[185]G. J. Kutcher, L. Coia, M. Gillin, W. F. Hanson, S. Leibel, R. J. Morton, J. R. Palta, J. A. Purdy, L. E. Reinstein, G. K. Svensson, M. Weller, and L. Wingfield, "Comprehensive QA for radiation oncology: Report of AAPM Radiation Therapy Committee Task Group 40," Med. Phys. **21**, 581–618 (1994).
[186]R. Nath, L. L. Anderson, J. A. Meli, A. J. Olch, J. A. Stitt, and J. F. Williamson, "Code of practice for brachytherapy physics: Report of the AAPM Radiation Therapy Committee Task Group No. 56," Med. Phys. **24**, 1557–1598 (1997).
[187]H. D. Kubo, G. P. Glasgow, T. D. Pethel, B. R. Thomadsen, and J. F. Williamson, "High dose-rate brachytherapy treatment delivery: Report of the AAPM Radiation Therapy Committee Task Group No. 59," Med. Phys. **25**, 375–403 (1998).
[188]J. Perez-Calatayud, F. Ballester, R. K. Das, L. A. DeWerd, G. S. Ibbott, A. S. Meigooni, Z. Ouhib, M. J. Rivard, R. S. Sloboda, and J. F. Williamson, "Dose calculation for photon-emitting brachytherapy sources with average energy higher than 50 keV: Report of the AAPM and ESTRO," Med. Phys. **39**, 2904–2929 (2012).
[189]A. Angelopoulos, P. Baras, L. Sakelliou, P. Karaiskos, and P. Sandilos, "Monte Carlo dosimetry of a new ^{192}Ir high dose rate brachytherapy source," Med. Phys. **27**, 2521–2527 (2000).
[190]C. S. Melhus and M. J. Rivard, "COMS eye plaque brachytherapy dosimetry simulations for ^{103}Pd, ^{125}I, and ^{131}Cs," Med. Phys. **35**, 3364–3371 (2008).
[191]M. J. Rivard, S.-T. Chiu-Tsao, P. T. Finger, A. S. Meigooni, C. S. Melhus, F. Mourtada, M. E. Napolitano, D. W. O. Rogers, R. M. Thomson, and R. Nath, "Comparison of dose calculation methods for brachytherapy of intraocular tumors," Med. Phys. **38**, 306–316 (2011).
[192]D. A. Low and J. F. Dempsey, "Evaluation of the gamma dose distribution comparison method," Med. Phys. **30**, 2455–2464 (2003).
[193]D. A. Low, J. M. Moran, J. F. Dempsey, L. Dong, and M. Oldham, "Dosimetry tools and techniques for IMRT," Med. Phys. **38**, 1313–1338 (2011).
[194]E. A. Bannon, Y. Yang, and M. J. Rivard, "Accuracy assessment of the superposition principle for evaluating dose distributions of elongated and curved ^{103}Pd and ^{192}Ir brachytherapy sources," Med. Phys. **38**, 2957–2963 (2011).
[195]J. Venselaar, H. Welleweerd, and B. Mijnheer, "Tolerances for the accuracy of photon beam dose calculations of treatment planning systems," Radiother. Oncol. **60**, 191–201 (2001).
[196]M. Stock, B. Kroupa, and D. Georg, "Interpretation and evaluation of the γ index and the γ index angle for the verification of IMRT hybrid plans," Phys. Med. Biol. **50**, 399–411 (2005).
[197]L. A. DeWerd, G. S. Ibbott, A. S. Meigooni, M. G. Mitch, M. J. Rivard, K. E. Stump, B. R. Thomadsen, and J. L. M. Venselaar, "A dosimetric uncertainty analysis for photon-emitting brachytherapy sources: Report of AAPM Task Group No. 138 and GEC-ESTRO," Med. Phys. **38**, 782–801 (2011).
[198]R. Mohan, C. Chui, and L. Lidofsky, "Differential pencil beam dose computation model for photons," Med. Phys. **13**, 64–73 (1986).
[199]A. Ahnesjö, P. Andreo, and A. Brahme, "Calculation and application of point spread functions for treatment planning with high energy photon beams," Acta Oncol. **26**, 49–56 (1987).
[200]R. Nath, L. Anderson, D. Jones, C. Ling, R. Loevinger, J. Williamson, and W. Hanson, "Specification of brachytherapy source strength: Report of AAPM Task Group No. 32," AAPM Report No. 21 (American Institute of Physics, New York, 1987).
[201]S. Nag, D. Beyer, J. Friedland, P. Grimm, and R. Nath, "American Brachytherapy Society (ABS) recommendations for transperineal permanent brachytherapy of prostate cancer," Int. J. Radiat. Oncol., Biol., Phys. **44**, 789–799 (1999).
[202]R. Kline and J. Earle, "Implications of TG-43 for dose prescription and calculation for I-125 eye plaques," Med. Phys. **23**, 1054 (1996) (abstract).

[203] J. F. Williamson, W. Butler, L. A. Dewerd, M. S. Huq, G. S. Ibbott, Z. Li, M. G. Mitch, R. Nath, M. J. Rivard, and D. Todor, "Recommendations of the American Association of Physicists in Medicine regarding the impact of implementing the 2004 Task Group 43 report on dose specification for ^{103}Pd and ^{125}I interstitial brachytherapy," Med. Phys. **32**, 1424–1439 (2005).

[204] M. J. Rivard, W. M. Butler, P. M. Devlin, J. K. Hayes Jr., R. A. Hearn, E. P. Lief, A. S. Meigooni, G. S. Merrick, and J. F. Williamson, "American Brachytherapy Society recommends no change for prostate permanent implant dose prescriptions using iodine-125 or palladium-103," Brachytherapy **6**, 34–37 (2007).